Revista Mexicana de Astronomía y Astrofísica, **47**, 235–253 (2011)

ON THE STELLAR AND BARYONIC MASS FRACTIONS OF CENTRAL BLUE AND RED GALAXIES

A. Rodríguez-Puebla,[1] V. Avila-Reese,[1] C. Firmani,[1,2] and P. Colín[3]

Received 2011 January 21; accepted 2011 April 14

RESUMEN

Con la técnica del empate de abundancias, las relaciones locales masa estelar y bariónica-masa de halo ($M_{\rm s}$–$M_{\rm h}$ y $M_{\rm b}$–$M_{\rm h}$) para galaxias *centrales* azules y rojas (GAs y GRs) se infieren por separado. Se hace uso de las funciones de masa estelar galáctica observadas de GAs y GRs y las respectivas relaciones masa de gas-$M_{\rm s}$. Las funciones de masa de halos asociados a las GAs y GRs centrales se toman de una descomposición adecuadamente obtenida de la función de halos distinguibles ΛCDM. Para $M_{\rm h} \gtrsim 10^{11.5}\ M_\odot$, la $M_{\rm s}$ de GRs tiende a ser mayor que la de GAs a una dada $M_{\rm h}$, pero no más que un factor ∼1.7. Para $M_{\rm h} \lesssim 10^{11.5}\ M_\odot$, esta tendencia se invierte. Para GAs (GRs): (a) el máximo de $f_{\rm s}$=$M_{\rm s}/M_{\rm h}$ es $0.021^{+0.016}_{-0.009}$ ($0.034^{+0.026}_{-0.015}$) y se alcanza a $\log(M_{\rm h}/M_\odot) = 12.0$ (= 11.9); (b) $f_{\rm s} \propto M_{\rm h}$ ($f_{\rm s} \propto {M_{\rm h}}^3$) hacia el lado de bajas masas, mientras que en el otro extremo $f_{\rm s} \propto {M_{\rm h}}^{-0.4}$ ($f_{\rm s} \propto {M_{\rm h}}^{-0.6}$). Las $f_{\rm b}$=$M_{\rm b}/M_{\rm h}$ de GAs y GRs son cercanas para $M_{\rm h} \gtrsim 10^{11.7}\ M_\odot$, y alcanzan valores máximos de $f_{\rm b} = 0.028^{+0.018}_{-0.011}$ y $f_{\rm b} = 0.034^{+0.025}_{-0.014}$. Hacia masas menores la dependencia de $f_{\rm b}$ sobre $M_{\rm h}$ es mucho más empinada para GRs que para GAs. Discutimos las diferencias encontradas para las relaciones $f_{\rm s}$–$M_{\rm h}$ y $f_{\rm b}$–$M_{\rm h}$ entre GAs y GRs a la luz de inferencias semi-empíricas de evolución galáctica.

ABSTRACT

Using the abundance matching technique, we infer the local stellar and baryonic mass-halo mass ($M_{\rm s}$–$M_{\rm h}$ and $M_{\rm b}$–$M_{\rm h}$) relations separately for *central* blue and red galaxies (BGs and RGs). The observational inputs are the SDSS central BG and RG stellar mass functions and the measured gas mass-$M_{\rm s}$ relations. For halos associated to central BGs, the distinct ΛCDM halo mass function is used and set up to exclude: (i) the observed group/cluster mass function and (ii) halos with a central major merger at resdshifts $z \leq 0.8$. For central RGs, the complement of this mass function to the total one is used. At $M_{\rm h} > 10^{11.5}\ M_\odot$, the $M_{\rm s}$ of RGs tend to be higher than those of BGs for a given $M_{\rm h}$, the difference not being larger than 1.7. At $M_{\rm h} < 10^{11.5}\ M_\odot$, this trend is inverted. For BGs (RGs): (a) the maximum value of $f_{\rm s} = M_{\rm s}/M_{\rm h}$ is $0.021^{+0.016}_{-0.009}$ ($0.034^{+0.026}_{-0.015}$) and it is attained at $\log(M_{\rm h}/M_\odot) = 12.0$ (= 11.9); (b) $f_{\rm s} \propto M_{\rm h}$ ($f_{\rm s} \propto {M_{\rm h}}^3$) at the low-mass end while at the high-mass end, $f_{\rm s} \propto {M_{\rm h}}^{-0.4}$ ($f_{\rm s} \propto {M_{\rm h}}^{-0.6}$). The baryon mass fractions, $f_{\rm b}$=$M_{\rm b}/M_{\rm h}$, of BGs and RGs reach maximum values of $f_{\rm b} = 0.028^{+0.018}_{-0.011}$ and $f_{\rm b} = 0.034^{+0.025}_{-0.014}$, respectively. At $M_{\rm h} < 10^{11.3}\ M_\odot$, the dependence of $f_{\rm b}$ on $M_{\rm h}$ is much steeper for RGs than for BGs. We discuss the differences found in the $f_{\rm s}$–$M_{\rm h}$ and $f_{\rm b}$–$M_{\rm h}$ relations between BGs and RGs in the light of semi-empirical galaxy evolution inferences.

Key Words: dark matter — galaxies: luminosity function, mass function

1. INTRODUCTION

The galaxy stellar and baryonic mass functions (*GSMF* and *GBMF*, respectively), inferred from the observed luminosity function and gas fraction-stellar mass ($f_{\rm g}$–$M_{\rm s}$) relation, contain key statistical in-

[1]Instituto de Astronomía, Universidad Nacional Autónoma de México, Mexico.
[2]Osservatorio Astronomico di Brera, Italy.
[3]Centro de Radioastronomía y Astrofísica, Universidad Nacional Autónoma de México, Mexico.

formation to understand the physical processes of galaxy formation and evolution. Within the context of the popular Λ Cold Dark Matter (ΛCDM) hierarchical scenario, dark matter halos are the sites where galaxies form and evolve (White & Rees 1978; White & Frenk 1991). Hence, a connection between *GBMF* or *GSMF* and the halo mass function (*HMF*) is expected. The result of such a connection is the galaxy stellar and baryonic mass-halo mass relations, $M_{\rm s}$–$M_{\rm h}$ and $M_{\rm b}$–$M_{\rm h}$, and their intrinsic scatters, both set by complex dynamical and astrophysical processes intervening in galaxy formation and evolution (see for recent reviews Baugh 2006; Avila-Reese 2007; Benson 2010). In this sense, the $M_{\rm b}/M_{\rm h}$ and $M_{\rm s}/M_{\rm h}$ ratios quantify the efficiency at which galaxy and star formation proceeds within a halo of mass $M_{\rm h}$. Therefore, the empirical or semi-empirical inference of the $M_{\rm b}$–$M_{\rm h}$ and $M_{\rm s}$–$M_{\rm h}$ relations and their scatters (locally and at other epochs) is nowadays a challenge of great relevance in astronomy.

For simplicity, in statistical studies like those related to the *GSMF*, galaxies are labelled by their mass alone. However, according to their observed properties, correlations, and evolution, galaxies show a very different nature, at least for the two major groups in which they are classified: the rotationally-supported disk star-forming (late-type) and the pressure-supported spheroid quiescent (early-type) galaxies. In the same way, the evolution of galaxies is expected to differ if they are centrals or satellites. The main intrinsic processes of galaxy evolution are associated to central galaxies, while satellite galaxies undergo several *extra* astrophysical processes because of the influence of the environment of the central galaxy/halo system in which they were accreted. Hence, if the $M_{\rm b}$–$M_{\rm h}$ or $M_{\rm s}$–$M_{\rm h}$ relations are used for constraining galaxy formation and evolution processes, these relations are separately required for at least the two main families of late- and early-type galaxies and should take into account whether the galaxy is central or satellite. Fortunately, in the last years there appeared several studies in which a decomposition of complete *GSMF*s by color, concentration or other easily measurable indicators of the galaxy type was carried out (e.g., Bell et al. 2003; Shao et al. 2007; Bernardi et al. 2010). Furthermore, in a recent work Yang, Mo, & van den Bosch (2009, hereafter YMB09) used the Sloan Digital Sky Survey (SDSS) data to obtain the *GSMF*s of both central and central + satellite galaxies separated in each case into blue and red objects.

With the advent of large galaxy surveys, a big effort has been made to constrain the $z \sim 0$ *total* $M_{\rm s}$–$M_{\rm h}$ relation (i) *directly* by estimating halo masses with galaxy-galaxy weak lensing, with kinematics of satellite galaxies or with X-ray studies; and (ii) *indirectly* by linking observed statistical galaxy properties (e.g., the galaxy stellar mass function *GSMF*, the two-point correlation function, galaxy group catalogs) to the theoretical *HMF* (for recent reviews and additional references see Moster et al. 2010; Behroozi, Conroy, & Wechsler 2010, hereafter BCW10; More et al. 2011). While the latter approach does not imply a measure-based determination of halo masses, it is simpler from a practical point of view, as it allows to cover larger mass ranges, and can be extended to higher redshifts than the former approach (see recent results in Conroy & Wechsler 2009; Moster et al. 2010; Wang & Jing 2010; BCW10). Besides, both the weak lensing and satellite kinematics methods in practice are (still) statistical in the sense that one needs to stack large number of galaxies in order to get sufficient signal-to-noise. This introduces a significant statistical uncertainty in the inferred halo masses.

The indirect approach for linking galaxy and halo masses spans a large variety of methods, among which the halo occupation distribution (Peacock & Smith 2000; Berlind & Weinberg 2002; Kravtsov et al. 2004) and the conditional luminosity function formalisms (Yang, Mo, & van den Bosch 2003; Yang et al. 2004) can be mentioned. These formalisms introduce *a priori* functional forms with several parameters that should be constrained by the observations. Therefore, the final inferred $M_{\rm s}$–$M_{\rm h}$ relation is actually model-dependent and yet sometimes poorly constrained due to degeneracies in the large number of parameters. A simpler and more empirical method –in the sense that it uses only the *GSMF* (or luminosity function) as input and does not require to introduce any model– has been found to give reasonable results. This indirect method, called the abundance matching technique (hereafter AMT; e.g., Marinoni & Hudson 2002; Vale & Ostriker 2004; Conroy, Wechsler, & Kravtsov 2006; Shankar et al. 2006; Conroy & Wechsler 2009; Baldry, Glazebrook, & Driver 2008; Guo et al. 2010; Moster et al. 2010; BCW10), is based on the assumption of a monotonic correspondence between $M_{\rm s}$ and $M_{\rm h}$; in the limit of zero scatter in the $M_{\rm s}$–$M_{\rm h}$ relation, the halo mass $M_{\rm h}$ corresponding to a galaxy of stellar mass $M_{\rm s}$, is found by matching the observed cumulative *GSMF* to the theoretical cumulative *HMF*.

In this paper we apply the AMT in order to infer the local $M_{\rm s}$–$M_{\rm h}$ relation for *central blue and red* galaxies separately, which requires as input *both* the

observed central blue and red *GSMF*s, taken here from YMB09. Note that in order to infer the $M_{\rm s}$–$M_{\rm h}$ relation of galaxy subpopulations (e.g., blue/red or central/satellite ones) solely from the overall *GSMF*, models for each subpopulation should be introduced, which greatly increases the uncertainty of the result. Regarding the *HMF*s to be matched with the corresponding observed central *GSMF*s, the theoretical *HMF* is decomposed into two functions –associated to halos hosting blue and red galaxies– based on empirical facts: blue galaxies are rare as central objects in groups/clusters of galaxies, and they should not have undergone late major mergers because of the dynamical fragility of disk (blue) galaxies. Nowadays, it is not clear whether or not the $M_{\rm s}$–$M_{\rm h}$ relation varies significantly with galaxy color or type. Previous studies that discussed this question were based on direct methods: the weak lensing (Mandelbaum et al. 2006) and satellite kinematics (More et al. 2011) techniques. The uncertainties in the results of these studies are still large, and can be subject to biases intrinsic to the sample selection and to effects of environment.

We also estimate here the galaxy baryon mass-halo mass relations, $M_{\rm b}$–$M_{\rm h}$[4], where $M_{\rm b}$= $M_{\rm s}$+ $M_{\rm g}$, by using the *GSMF*s combined with average observational determinations of the galaxy gas mass, $M_{\rm g}$, as a function of $M_{\rm s}$. The galaxy baryonic mass fraction, $f_{\rm b}$= $M_{\rm b}/M_{\rm h}$, and its dependence on mass is important for constraining models and simulations of galaxy evolution, and is also a key input for some approaches, implemented to model the most generic population of galaxies, namely *isolated (central) disk galaxies* (e.g., Mo, Mao, & White 1998; Firmani & Avila-Reese 2000; van den Bosch 2000; Stringer & Benson 2007; Dutton et al. 2007; Gnedin et al. 2007; Dutton & van den Bosch 2009). In these and other studies, it was shown that several disk galaxy properties, correlations, and their scatters depend (or are constrained) by $f_{\rm b}$. In a similar way, the $f_{\rm b}$–$M_{\rm h}$ dependence is expected to play some role in the results of structural and dynamical models of spheroid-dominated galaxies.

In § 2 we describe the method and the data input. The stellar/baryon mass-halo mass relations for the total, blue and red (sub)samples are presented in § 3. In § 4 we compare our results with other observational works, and discuss whether they are consistent or not with expectations of semi-empirical inferences. The summary and our conclusions are given in § 5.

[4]We assume that the galaxy baryonic mass is included in the halo (virial) mass $M_{\rm h}$.

2. THE METHOD

The AM statistical technique is based on the hypothesis of a one-to-one monotonic increasing relationship between $M_{\rm s}$ (or $M_{\rm b}$) and $M_{\rm h}$. Therefore, by matching the *cumulative* galaxy stellar and halo mass functions, for a given $M_{\rm s}$ a unique $M_{\rm h}$ is assigned:

$$\int_{M_{\rm h}}^{\infty} \phi_h(M'_h)dM'_h = \int_{M_{\rm s}}^{\infty} \phi_s(M'_s)dM'_s, \qquad (1)$$

where ϕ_h is the overall *HMF* (distinct + subhalos) and ϕ_s is the overall *GSMF*; *distinct* halos are those not contained inside more massive halos. It is reasonable to link central galaxies with distinct halos. Therefore, in the case of using the *GSMF* for only central galaxies, the distinct *HMF* should be used for the matching. Since the main purpose of this paper is the inference of the $M_{\rm s}$–$M_{\rm h}$ (and the corresponding $M_{\rm b}$–$M_{\rm h}$) relation for blue (red) galaxies, (i) a *GSMF* that separates galaxies by color is necessary (the data to be used here are discussed in § 2.1), and (ii) a criterion to select the halos that will likely host blue (red) galaxies shall be introduced (see § 2.2.1).

In this paper we will not carry out an exhaustive analysis of uncertainties in the inference of the $M_{\rm s}$–$M_{\rm h}$ relation with the AMT. This was extensively done in BCW10 (see also Moster et al. 2010). In BCW10 the uncertainty sources are separated into three classes: uncertainties (i) in the observational inference of *GSMF*, (ii) in the dark matter HMF, which includes uncertainties in the cosmological parameters, and (iii) in the matching process arising primarily from the intrinsic scatter between $M_{\rm s}$ and $M_{\rm h}$.

2.1. *Galaxy and Baryonic Stellar Mass Functions*

In the last years, complete galaxy luminosity functions (and therefore, *GSMF*s) were determined for local samples covering a large range of luminosities (masses). The stellar mass is inferred from (multi) photometric and/or spectral data (i) by using average stellar mass-to-light ratios, depending only on color (inferred from application of stellar population synthesis –SPS– models to galaxy samples with independent mass estimates, e.g., Bell et al. 2003), or (ii) by applying directly the SPS technique to each sample galaxy, when extensive multi-wavelength and/or spectral information is available.

In both cases, a large uncertainty is introduced in the inference of $M_{\rm s}$ due to the uncertainties in the IMF, stellar evolution, stellar spectral libraries, dust extinction, metallicity, etc. Bell et al. (2003) estimated a scatter of ≈0.1 dex in their $M_{\rm s}/L$ ratios

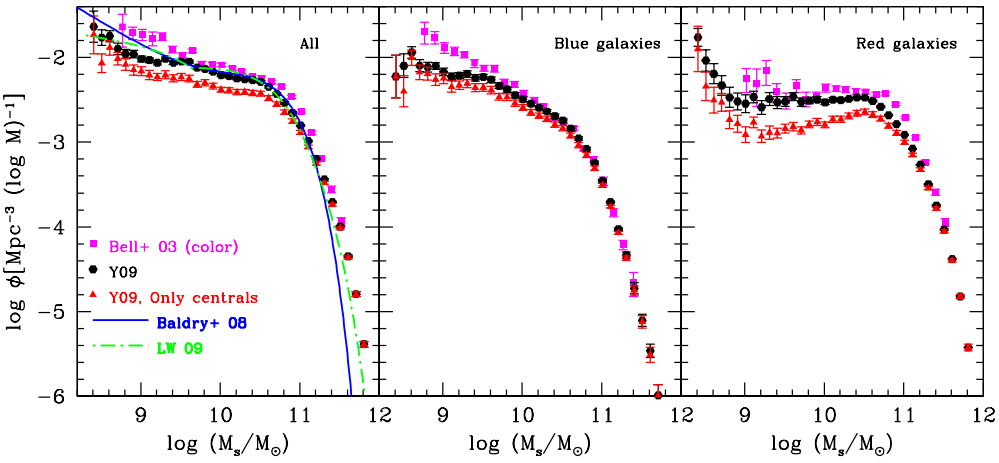

Fig. 1. Left panel: Different local *GSMF*s for *all* galaxies. The reported data in Bell et al. (2003, pink squares) and YMB09 (black hexagons) are plotted directly, while for Baldry et al. (2008, blue solid line) and Li & White (2009, dot-dashed green line), the best fits these authors find to their samples are plotted. Red triangles show the data from YMB09 corresponding to the *GSMF* of central-only galaxies. Middle and right panels: Data corresponding to the decomposition of the *GSMF* into blue and red galaxies, respectively, from Bell et al. (2003) and for the all and central-only galaxies from YMB09. The color figure can be viewed online.

in infrared bands. Conroy, Gunn, & White (2009) carried out a deep analysis of propagation of uncertainties in SPS modelling and concluded that $M_{\rm s}$ at $z \sim 0$ carry errors up to ∼0.3 dex (but see Gallazzi & Bell 2009). Here, we will consider an overall systematic uncertainty of 0.25 dex in the $M_{\rm s}$ determination (see BCW10).

Most of the current local *GSMF*s were inferred from 2dF Galaxy Redshift Survey, Two Micron All-Sky Survey (2MASS) and SDSS (e.g., Cole et al. 2001; Bell et al. 2003; Baldry et al. 2006). The low-mass completeness limit due to missing low surface brightness galaxies occurs at $\sim 10^{8.5}$ $M_{\rm s}$ (Baldry et al. 2008). An upturn of the *GSMF* close to this end (below $M_{\rm s} \sim 10^{9}$ $M_{\odot}$) was confirmed in several recent works (Baldry et al. 2008; YMB09; Li & White 2009). Due to this upturn, a better fit to the *GSMF*s is obtained by using a double or even triple Schechter function. Since the low-mass end of the *GSMF* is dominated by late-type galaxies, this upturn plays an important role in the $M_{\rm s}$–$M_{\rm h}$ relation of late-type galaxies at low masses.

For our purposes, observational works where the *GSMF* is decomposed into late- and early-types galaxies are required. Such a decomposition has been done, for example, in Bell et al. (2003), who combined 22679 SDSS Early Data Release and 2MASS galaxies, and used two different criteria, color and concentration, to split the sample into two types of galaxies. A much larger sample taken from the NYU-VAGC based on the SDSS DR4 has been used by YMB09 (see also Yang, Mo, & van den Bosch 2008), who split the sample into *blue and red* subsamples according to a criterion in the ${}^{0.1}(g-r)-M_r$ diagram. In both works, $M_{\rm s}$ is calculated from the $r-$band magnitude by using the corresponding color-dependent $M_{\rm s}/L_r$ ratio given in Bell et al. (2003). In YMB09 each color subsample is in turn separated into central and satellite galaxies according to their memberships in the constructed groups, where the central galaxy is defined as the most massive one in the group and the rest as satellite galaxies.

In Figure 1, the Bell et al. (2003) and YMB09 *GSMF*s are reproduced by using the data sets reported in these papers. In the left panel, the full samples from each work (solid squares and solid hexagons, respectively) are plotted, as well as the case of central-only galaxies from YMB09 (solid triangles); both *GSMF*s and the other ones plotted in this figure are normalised to $h = 0.7$ and to a Chabrier (2003) IMF. In the central and right panels, the corresponding blue (late-type) and red (early-type) sub-samples are plotted with the same symbols as in the left panel. For the Bell et al. (2003) sub-samples, only those separated by their color criterion are plotted. Both *GSMF*s corresponding to the full and blue sub-samples are in good agreement for $M_{\rm s} \gtrsim 10^{9.5}$ $M_{\odot}$. For lower masses, the Bell et al. (2003) *GSMF*'s are higher. On one hand, the Bell et al. (2003) sample is much smaller than the

YMB09 one (therefore its cosmic variance is more significant). On the other hand, the redshift completeness and M_s limit in YMB09 are treated with updated criteria.

In Figure 1 we also plot fits to the overall *GSMF* presented in Baldry et al. (2008, double Schechter function, solid blue line) and in Li & White (2009, triple Schechter function, dashed green line) for new SDSS releases and by using directly SPS models to estimate M_s for each galaxy. These fits agree well with the YMB09 data in the mass range $9.2 \lesssim \log(M_s/M_\odot) \lesssim 11.2$. For smaller masses, the Baldry et al. (2008) fit tends to be steeper while the Li & White (2009) fit tends to be shallower than the YMB09 data. For larger masses, both fits decrease faster with M_s than the YMB09 data. All these (small) differences are due to the different methods used to estimate M_s, as well as the different volumes and limit corrections of the samples (see Baldry et al. 2008, YMB09, and Li & White 2009 for discussions).

The split into two colors of the sample used by YMB09 is a rough approximation to the two main families of disk- and spheroid-dominated galaxies. It is well known that the morphological type correlates with the galaxy color, though with a large scatter. There is for example a non-negligible fraction of galaxies (mostly highly inclined) that are red but of disk-like type (e.g., Bernardi et al. 2010). However, given that here we consider a partition of the overall sample just in two groups, we believe that it is reasonable to assume as a first approximation that the color criterion for the partition will provide at this level a result similar to that of a morphological criterion.

For the YMB09 sample, the blue and red galaxies are ≈55% and ≈45%, respectively, for $M_s \gtrsim 3 \times 10^8\ M_\odot$. Red galaxies dominate the total *GSMF* at large masses. At $M_s \approx 2 \times 10^{10}\ M_\odot$ the abundances of red and blue galaxies are similar and at lower masses the latter are increasingly more abundant than the former as M_s is smaller. For $M_s \lesssim 10^9\ M_\odot$, the abundance of red galaxies, mainly central ones, steeply increases towards smaller masses. The existence of this peculiar population of faint central red galaxies is discussed in YMB09. Wang et al. (2009) suggested that these galaxies are hosted by small halos that have passed through their massive neighbors, and the same environmental effects that cause satellite galaxies to become red are also responsible for the red colors of such galaxies. However, as these authors showed, even if the environmental effects work, there are in any case over 30% of small halos that are completely isolated, so that these effects cannot be invoked for them.

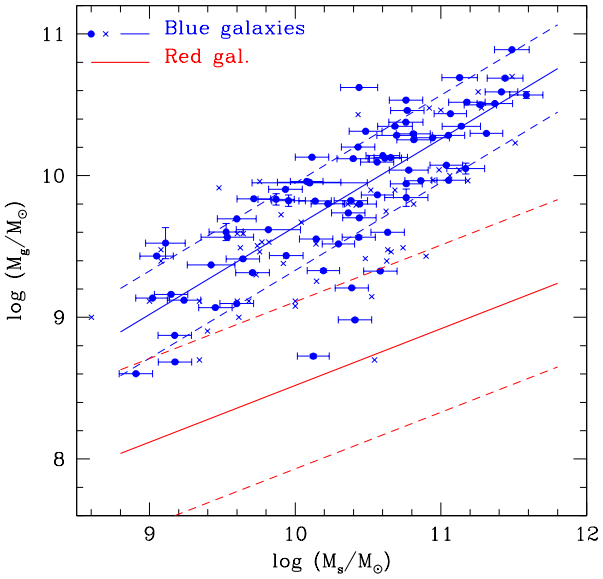

Fig. 2. Gas mass vs stellar mass for a sample of disk high and low surface brightness galaxies collected and homogenised by Avila-Reese et al. (2008, blue dots with error bars) and for a sample of disk galaxies presented by McGaugh (2005, blue crosses). The solid blue line is the orthogonal linear doubly-weighted regression to the data from the former authors and the dashed lines show an estimate of the intrinsic scatter around the fit. The solid red line is an estimate of the M_g–M_s correlation for red galaxies using our fit to blue galaxies and the ratio of blue-to-red atomic gas fraction determined in Wei et al. (2010), see text. The color figure can be viewed online.

In the YMB09 sample, around 70% of the galaxies are central. As mentioned in the § 1, the inference of the M_s–M_h relation for central-only galaxies is important for studies aimed to constrain galaxy formation and evolution in general; satellite galaxies are interesting on its own but they lack generality because their evolution and properties are affected by extra environmental processes.

In what follows, the YMB09 *GSMF* provided in tabular form and split into blue/red and central/satellite galaxies will be used for applying the AMT. Our main goal is to infer the M_s–M_h relation for central blue (late-type) and red (early-type) galaxies.

We will infer also the corresponding M_b–M_h (baryonic) relations. The blue and red *GBMF*s are estimated from the blue and red *GSMF*s, respectively, where in order to pass from M_s to M_b, the cool (atomic and molecular) gas mass, M_g, corre-

sponding on average to a given $M_{\rm s}$ is taken from the empirical blue and red $M_{\rm g}$–$M_{\rm s}$ relations. In Figure 2 a compilation of observational estimates is plotted in the $M_{\rm s}$–$M_{\rm g}$ plane for a sample of disk galaxies that includes low surface brightness galaxies from Avila-Reese et al. (2008; blue dots with error bars; they added H_2 mass contribution by using an estimate for the H_2-to-HI mass ratio as a function of galaxy type), and for another galaxy sample from McGaugh (2005; blue crosses; no H_2 contribution is considered and their dwarf galaxies were excluded). An orthogonal linear doubly-weighted regression to the data from Avila-Reese et al. (2008) gives:

$$\frac{M_{\rm g}}{10^{10}M_{\odot}} = 0.43 \times \left(\frac{M_{\rm s}}{10^{10}M_{\odot}}\right)^{0.62}. \qquad (2)$$

This fit is plotted in Figure 2 with its corresponding estimated scatter (≈0.3 dex; blue solid and dashed lines). This is the relation and its scatter used to calculate $M_{\rm b}$ and the blue *GBMF*. A similar relation has been inferred by Stewart et al. (2009). The gas fractions in red galaxies are much smaller than in blue galaxies. For sub-samples of blue and red galaxies, Wei et al. (2010) reported for each one the atomic gas fractions versus $M_{\rm s}$ (molecular gas was not included). The ratio of their fits to these data as a function of $M_{\rm s}$ is used here to estimate from equation 2 (blue galaxies) the corresponding average $M_{\rm g}$ for red galaxies as a function of $M_{\rm s}$. The red solid line shows the obtained relationship. As an approximation to the scatter (short-dashed lines), the average scatter reported for red galaxies in Wei et al. (2010) is adopted here.

2.2. *Halo and sub-halo mass functions*

A great effort has been made in the last decade to determine the *HMF* at $z = 0$ and at higher redshifts by means of N-body cosmological simulations. A good fit to the results, at least for low redshifts, is the universal function derived from a Press-Schechter formalism (Press & Schechter 1974) generalized to the elliptical gravitational collapse (Sheth & Tormen 1999, hereafter S-T). In fact, Tinker et al. (2008) have shown that at a high precision level, the *HMF* may change for different cosmological models and halo mass definitions as well as a function of z. For our purposes and for the cosmology used here, the S-T approximation provides a good description of the $z = 0$ *HMF* of distinct halos:

$$\phi_h(M_h)dM_h = A\left(1+\frac{1}{\nu^{2q}}\right)\sqrt{\frac{2}{\pi}}\frac{\bar{\rho}_M\nu}{M_h^2}\left|\frac{d\ln\sigma}{d\ln M_h}\right|\exp\left[-\frac{\nu^2}{2}\right]dM_h, \qquad (3)$$

where $A = 0.322$, $q = 0.3$, $\nu^2 = a(\delta_c/D(z)\sigma(M_{\rm h}))$ with $a = 0.707$; $\delta_c = 1.686\Omega_m^{0.0055}$ is the linear threshold in the case for spherical collapse in a flat universe with cosmological constant, $D(z)$ is the growth factor and $\sigma(M_{\rm h})$ is the mass power spectrum variance of fluctuations linearly extrapolated to $z = 0$. The halo (virial) mass, $M_{\rm h}$ is defined in this paper as the mass enclosed within the radius where the overdensity is $\bar{\rho}_{\rm vir} = \Delta$ times the *mean matter* density, $\bar{\rho}_M$; $\Delta \approx 340$ according to the spherical collapse model for the cosmology used here. The cosmological parameters assumed here are close to those of WMAP5 (Komatsu et al. 2009): $\Omega_M = 0.27, \Omega_\Lambda = 1 - \Omega_m = 0.73, h = 0.70, \sigma_8 = 0.8$.

The distinct *HMF* should be corrected when a *GSMF* corresponding to *all* galaxies is used in the AMT. In this case, satellite galaxies are included in the *GSMF*. Therefore, subhalos should be taken into account in the *HMF*. The subhalo fraction is no more than ≈20% of all the halos at $z = 0$ (e.g., Shankar et al. 2006; Conroy et al. 2006; Giocoli et al. 2010; BCW10). When necessary, we correct the S-T *HMF* for (present-day) subhalo population by using the fitting formula to numerical results given in Giocoli et al. (2010):

$$\frac{dn(m_{\rm sub})}{d\ln m_{\rm sub}} = A_0 m_{\rm sub}^{\eta-1}\exp\left[-\left(\frac{m_{\rm sub}}{m_0}\right)^{\gamma}\right], \qquad (4)$$

with $\eta = 0.07930$, $\log A_0 = 7.812$, $\log(m_0/M_{\odot}) = 13.10$ and $\gamma = 0.407$.

The upper panel of Figure 3 shows the (distinct) S-T *HMF* (solid line), the sub-halo *HMF* (short-long-dashed line), and the distinct+subhalo *HMF* (dash-dotted line). The correction by sub-halos in the abundance is small at low masses and negligible at high masses. When the *GSMF* refers only to central galaxies –which is the case in this paper– then it is adequate to use the distinct *HMF* for the AMT, i.e. *the subhalo abundance correction is not necessary.*

2.2.1. *Halos hosting blue and red galaxies*

In the AMT, the cumulative *GSMF* and *HMF* are matched in order to link a given $M_{\rm s}$ to $M_{\rm h}$. When a subsample of the total *GSMF* is used –as is the case for inferring the $M_{\rm s}$–$M_{\rm h}$ relation of only late- or early-type galaxies– it would not be correct to use the total *HMF* for the matching. This function, in the ignorance of which is the mass function of halos hosting blue (red) galaxies, at least should be re-normalised (decreased uniformly) by the same fraction corresponding to the decrease of the subsample *GSMF* with respect to the total *GSMF*. In

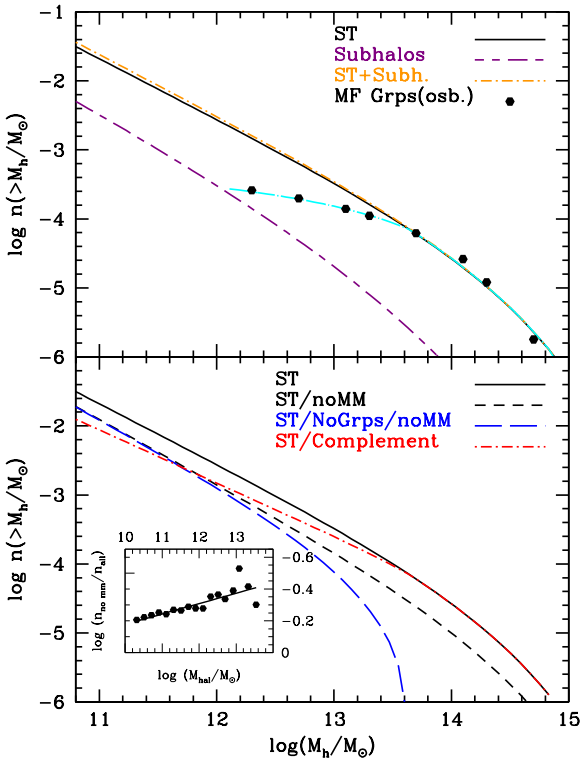

Fig. 3. Upper panel: Distinct S-T *HMF* for the cosmology adopted in this paper (solid black line), sub-halo mass function at $z = 0$ according to Giocoli et al. (2010, short-long-dashed purple line), and the sum of both (dot-dashed orange line). The solid dots are measures of the group/cluster mass function according to Heinämäki et al. (2003) and adequately corrected to our definition of virial halo mass; the dot-long-dashed cyan line is a eye-fit to the data. Lower panel: The same distinct S-T *HMF* (solid black line) shown in the upper panel but (i) excluding the halos that suffered late major mergers –since $z = 0.8$– (short-dashed black line) and (ii) excluding these halos and those of observed groups/clusters (long-dashed blue line). The latter is the *HMF* to be assigned to the sub-sample of central blue galaxies. The complement of this function to the total (S-T) one (dot-dashed red line) is the *HMF* to be assigned to the sub-sample of central red galaxies. The inset shows the ratio of number densities of halos that did not suffer major mergers since $z = 0.8$ to all the (distinct) halos according to measures in a cosmological N-body simulation (Colín et al. 2011, in preparation, see text). The fit to this ratio (solid line in the inset) is what has been used to correct the S-T *HMF* for halos thad did not suffer late major mergers. The color figure can be viewed online.

YMB09, ≈55% (≈45%) of the galaxies are in the blue (red) sub-samples for $M_{\rm s} \gtrsim 3 \times 10^8\ M_\odot$. We may go one step further by proposing general observational/physical conditions for halos to be the hosts of blue (late-type) or red (early-type) galaxies. Note that the division of galaxies we do here is quite broad –just into two groups– and therefore very general conditions are enough.

Halos that host central blue and red galaxies are expected to have (i) a different environment, and (ii) a different merger history. We take into account these two factors in order to roughly estimate the *HMF* of those halos that will host today central blue and red galaxies.

Environment.- Blue (late-type) galaxies are rare in the centers of groups and clusters of galaxies (high-density environments; e.g., Norberg et al. 2001; Zehavi et al. 2005; Li et al. 2006; de Lapparent & Slezak 2007; Padilla, Lambas, & González 2010; Blanton & Moustakas 2009, and references therein). For example, in the SDSS YMB09 sample that we use here (see also Weinmann et al. 2006), among the groups with 3 or more members, the fraction of those with a central blue galaxy is only ≈20%, and most of these central galaxies have actually low masses. Therefore, cluster- and group-sized halos (more massive than a given mass) cannot be associated to central blue galaxies when using the AMT. This means that the halo mass function of groups/clusters of galaxies should be excluded from the theoretical *HMF* (Shankar et al. 2006).

Heinämäki et al. (2003) determined the *HMF* of groups with 3 or more members and with a number density enhancement $\delta n/n \geq 80$ from the Las Campanas Redshift Survey. The authors estimated the corresponding group virial mass on the basis of the line-of-sight velocity and harmonic radius of the group, in such a way that this mass was defined at the radius where $\delta n/n = 80$. The observational galaxy overdensity $\delta n/n$ is related to the mass overdensity $\delta\rho/\rho$ roughly through the bias parameter b: $\delta\rho/\rho = (1/b) \times \delta N/N$, where $b \approx 1/\sigma_8$ (Martínez et al. 2002). Hence, for $\sigma_8 = 0.8$, $\delta\rho/\rho \approx 64$; since the group selection was carried out in Tucker et al. (2000), where an Einstein-de Sitter cosmology was used, then $\rho = \rho_{\rm crit}$ in this case. In our case, the halo virial mass is defined at the radius where $\delta\rho/\rho \approx 340$ (see § 2.2); in terms of $\rho_{\rm crit}$, our overdensity is $340 \times \Omega_M = 92$. Therefore, the halo virial masses in Heinämäki et al. (2003) should be slightly larger than those used here. For the NFW halos of masses larger than $\sim 10^{13}\ M_\odot$, the differences are estimated to be factors of 1.10–1.20. We correct the group masses of Heinämäki et al. (2003) by 15%. In the upper panel of Figure 3, the corrected group (halo) mass function is reproduced (solid dots) and a eye-fit to them is plotted (dot-dashed cyan line).

Merger history.- Disk (blue, late-type) galaxies are dynamically fragile systems and thus they are not expected to survive strong perturbations such as those produced in major mergers or close interactions. However, as several theoretical studies have shown (e.g., Robertson et al. 2004; Governato, Mayer, & Brook 2008), when the mergers are gas-rich ('wet') and/or occur at early epochs (in fact, both facts are expected to be correlated), it is highly probable that a gaseous disk is regenerated or formed again with the late accreted gas. Therefore, a reasonable restriction for halos that will host disk galaxies is that they did not undergo *central* major mergers since a given epoch (at earlier epochs, while the central major merger may destroy the disk, a new gaseous disk can be formed later on). Based on numerical simulations, Governato et al. (2008) suggested that a 'wet' major merger of disk galaxies at $z \sim 0.8$ has still a non-negligible probability of rebuilding a significant disk by $z \sim 0$. We will assume here that halos whose *centers* have a major merger at $z < 0.8$ will not host a disk galaxy.

In Colín et al. (2011, in preparation) the present-day abundance fraction of halos with no *central* major merger since $z = 0.8$ was measured as a function of $M_{\rm h}$ from an N-body ΛCDM cosmological high-resolution simulation with $\Omega_m = 0.24$, $\Omega_\Lambda = 0.76$, and $\sigma_8 = 0.75$ (box size and mass per particle of 64 h^{-1} Mpc and $1.64 \times 10^7 h^{-1}$ $M_\odot$, respectively). The friends-of-friends (FOF) method with a linking-length parameter of 0.17 was applied for identifying halos. The mass ratio to define a major merger was $q = M_{\rm h,2}/M_{\rm h,1} > 0.2$ and the merger epoch was estimated as the time when the center of the accreted halo arrived at the center of the larger halo by dynamical friction; this epoch is calculated as the cosmic time when both FOF halos have "touched" plus the respective dynamical friction (merging) time as given by the approximation of Boylan-Kolchin, Ma, & Quataert (2008). The fraction of halos that did not suffer a major merger since $z = 0.8$ with respect to all the halos as a function of $M_{\rm h}$ measured in Colín et al. (2011, in preparation) is used here to correct our distinct S-T *HMF*. This measured fraction is shown in the inset in the lower panel of Figure 3; the solid line is a linear fit by eye in the log-log plot: $\log(n_{\rm noMM}/n_{\rm all}) = 0.472 - 0.065\log(M_{\rm h}/M_\odot)$. As it is seen, the fraction slightly decreases with mass, which is consistent with the idea that larger mass halos are assembling later with a significant fraction of their masses being acquired in late major mergers. After the correction mentioned above, we get the mass function of halos that did not suffer a central major merger ($q > 0.2$) since $z = 0.8$ (short-dashed black line in the lower panel of Figure 3).

The final corrected HMFs.- The function obtained after (i) subtracting from the distinct S-T *HMF* the group mass function and (ii) excluding halos that did not suffer a late central major merger is plotted in Figure 3 (blue long-dashed line). This mass function is proposed here to correspond to halos that today host blue galaxies. The overall number fraction of these halos with respect to the distinct ones (described by the S-T *HMF*) is ∼58%, which is roughly consistent with the fraction of blue galaxies in the YMB09 sample. The *HMF* corresponding to the complement is plotted in Figure 3 as the red dot-dashed curve. By exclusion, this *HMF* will be associated with the *GSMF* of the red central galaxy sub-sample for deriving the $M_{\rm s}$–$M_{\rm h}$ relation of red galaxies.

3. RESULTS

3.1. *The overall, central, and satellite stellar-halo mass relations*

In Figure 4, the $M_{\rm s}$–$M_{\rm h}$ relation obtained by using the Li & White (2009) *GSMF* (see § 2.1 and Figure 1) and the S-T *HMF* corrected to include sub-halos is plotted (long-dashed blue line). The relation given by BCW10, who also used as input the Li & White (2009) *GSMF*, is shown (short-dashed red line). Both curves are almost indistinguishable, showing an excellent consistency of our results with those of BCW10, in spite of the differences in some of the methodological aspects.

Further, we plot in Figure 4 the $M_{\rm s}$–$M_{\rm h}$ relation as above but using now the total YMB09 *GSMF* (dot-dashed pink line). This relation is similar to the one inferred using the Li & White (2009) *GSMF*. For $\log(M_{\rm h}/M_\odot) \gtrsim 12$, the former slightly shifts with mass to higher values of $M_{\rm s}$ for a given $M_{\rm h}$ than the latter (at $\log(M_{\rm h}/M_\odot) = 13.5$ the difference is no larger than 0.08 dex in $\log M_{\rm s}$). Such a shift is explained by the (small) systematical difference between the YMB09 and Li & White (2009). *GSMF*s at masses larger than $\log(M_{\rm s}/M_\odot) \sim 11$ (see § 2.1 and Figure 1).

In Figure 4, the $M_{\rm s}$–$M_{\rm h}$ relations given in Baldry et al. (2008, dot-dashed orange line), Moster et al. (2010, short-long-dashed line) and Guo et al. (2010, dotted green line) are also plotted. When necessary, we have corrected the stellar masses to the Chabrier IMF, and the halo masses to the definition of virial mass used here (see § 2.2). As mentioned above, Baldry et al. (2008) corrected their *HMF* to exclude groups/clusters of galaxies (something that we do

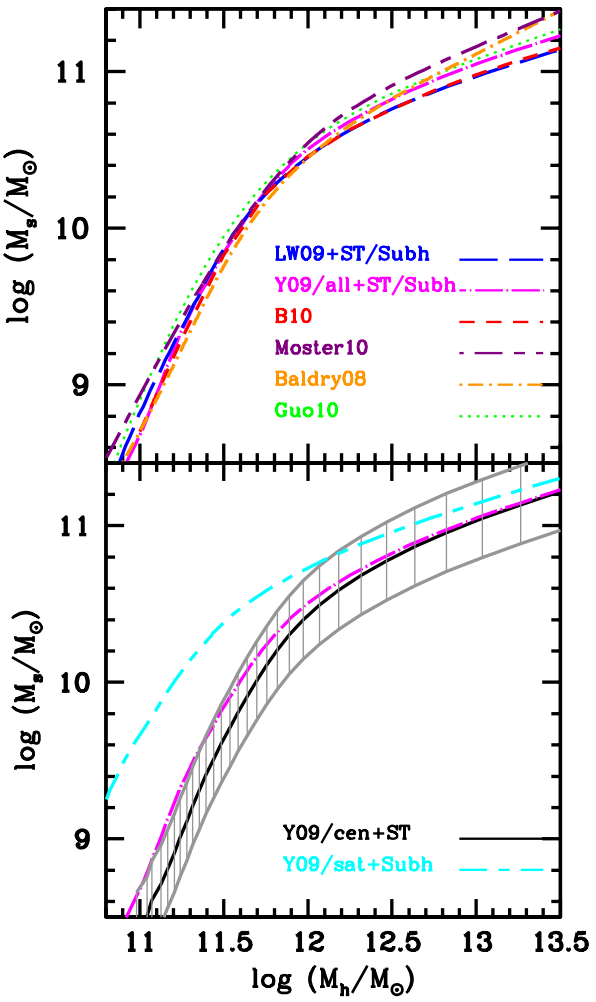

Fig. 4. Upper panel: Stellar mass vs halo mass as inferred here by using the Li & White (2009) overall *GSMF* and the S-T *HMF* increased by the subhalo population (long-dashed blue line) to be compared with the BCW10 inference, who used the same *GSMF* (short-dashed red line). The dot-dashed pink line shows the same M_s vs M_h inference but using the overall YMB09 *GSMF*. Different determinations of the overall M_s–M_h relation by other authors (indicated in the panel), who took into account in different ways the issue of group/cluster masses (see text) are also plotted. Lower panel: Same M_s–M_h relation as in the upper panel (dot-dashed pink line) but for the central-only YMB09 *GSMF* and the S-T (distinct) *HMF* (solid line). The grey curves connected by vertical lines show the estimated 1σ uncertainty for the latter case. The M_s–M_h relation inferred for the only satellite YMB09 *GSMF* and the Giocoli et al. (2010) $z = 0$ sub-halo mass function is plotted as a short-long-dashed cyan line. The color figure can be viewed online.

but only for the central blue galaxies, see § 2.2.1 and the result below). As seen in Figure 4, their correction produces a steeper M_s–M_h relation at the high-mass side than in our case. Moster et al. (2010) and Guo et al. (2010) constrained the M_s–M_h relation by assigning stellar masses to the halos and subhalos of an N-body cosmological simulation in such a way that the total *GSMF* was reproduced. Therefore, by construction, their M_s–M_h relations take into account the group/cluster halo masses issue. The M_s–M_h relations in both works are also slightly steeper than ours at high masses but shallower on average than that of Baldry et al. (2008). Note that in BCW10 the scatter in M_s at fixed M_h was taken into account but the group/cluster halo masses issue was not.

The M_s–M_h relation using the YMB09 *GSMF* only for central galaxies and the distinct (S-T) *HMF* is plotted in the lower panel of Figure 4 (solid black line). At large masses, this relation is quite similar to that for all galaxies/satellites and halos/subhalos (dot-dashed pink line). This is because at large masses the great majority of galaxies are centrals and the correction for sub-halos is negligible (see Figures 1 and 3). At lower masses, the exclusion of satellites and sub-halos implies a lower M_s for a given M_h. This is because the *GSMF* decreases more than the *HMF* as the mass is smaller when passing from the total (galaxy and halo) samples to the central-only galaxy/distinct halo samples. The physical interpretation of this result could be that satellite galaxies of a given M_s have less massive halos than central galaxies, due to tidal stripping. The M_s–M_h relation derived only for the satellites YMB09 *GSMF* and the Giocoli et al. (2010) $z = 0$ sub-halo *HMF* is plotted in the lower panel of Figure 4 (short-long-dashed cyan line).

3.1.1. *Uncertainties*

The uncertainty (standard deviation) in the M_s–M_h relation obtained using the YMB09 central *GSMF* and the distinct S-T *HMF* (solid line), is plotted in Figure 4 (grey curves connected by vertical lines). As remarked in § 2, we did not take into account all possible uncertainty sources in the M_s–M_h relation but have just considered the two following ones:

(i) The systematic uncertainty in stellar mass estimates, which is an uncertainty in the *GSMF*. We assume for this uncertainty a scatter of 0.25 dex (Gaussian-distributed) independent of mass, and propagate it to the M_s–M_h relation (it is by far the dominant source of error in the relation obtained with the AMT, see below and BCW10).

(ii) The intrinsic scatter in stellar mass at a fixed halo mass, which is an uncertainty in the process

of matching abundances. To take into account this scatter in $M_{\rm s}$ at fixed $M_{\rm h}$ a probability density distribution should be assumed. The convolution of this distribution with the true or intrinsic *GSMF* gives the measured *GSMF*. The cumulative true *GSMF* is then the one used for the AM (BCW10). The observational data allow to estimate the scatter in luminosity (or $M_{\rm s}$) and to date it appears to be independent of $M_{\rm h}$ (More et al. 2009; YMB09). In BCW10 a log-normal mass-independent scatter in $M_{\rm s}$ of 0.16 ± 0.04 is assumed. Here, we follow the overall procedure of BCW10 for taking into account this scatter.

We also explored the effect of (iii) the statistical uncertainty in the number density of the *GSMF* (as given in YMB09), but we found that the effect is negligible as compared to the one produced by item (i) (see also BCW10, their § 4.3.1). The effect of the intrinsic scatter in $M_{\rm s}$ for a given $M_{\rm h}$ is also very small in the overall scatter of the $M_{\rm s}$–$M_{\rm h}$ relation but it affects the high mass end of the calculated $M_{\rm s}$–$M_{\rm h}$ relation, where both the *GSMF* and *HMF* decay exponentially, since there are more low mass galaxies that are scattered upward than high mass galaxies that are scattered downward (BCW10). For instance, at $M_{\rm h} = 10^{13.5}\ M_{\odot}$, the stellar mass after including this scatter is 1.2 times smaller. The contribution from all other sources of error, including uncertainties in the cosmological model, is much smaller, ranging from 0.02 to 0.12 dex at $z = 0$.

From Figure 4 we see that the 1σ uncertainty in the $M_{\rm s}$–$M_{\rm h}$ relation is approximately 0.25 dex in log$M_{\rm s}$ without any systematic dependence on $M_{\rm h}$, in good agreement with previous results (BCW10; Moster et al. 2010). This uncertainty is larger than the differences between the $M_{\rm s}$–$M_{\rm h}$ average relations found by different authors, including those that use the indirect AMT but with different *GSMF*s, methodologies, and corrections, and those who use more sophisticated formalisms (see for comparisons and discussions BCW10 and More et al. 2011). On one hand, this shows that most methods and recent studies aimed at relating halo masses to observed galaxies as a function of their stellar masses are converging to a relatively robust determination. On the other hand, this result suggests that attaining a higher precision in estimating $M_{\rm s}$ from observations is the crucial task for lowering the uncertainty in the inference of the $M_{\rm s}$–$M_{\rm h}$ relation.

3.2. *The stellar-halo mass relations for central blue and red galaxies*

The upper and lower left panels of Figure 5 show the mean $M_{\rm s}$–$M_{\rm h}$ and $f_{\rm s}$–$M_{\rm h}$ relations for: all central galaxies (solid line, as in Figure 4), central blue (short-dashed line), and central red (long dashed line) galaxies. In order to infer these relations for blue galaxies, the central blue YMB09 *GSMF* and the distinct (S-T) *HMF* corrected for excluding halos (i) associated to observed groups/clusters of galaxies and (ii) that suffered central major mergers since $z = 0.8$ (see § 2.2.2) were used. In the case of red galaxies, the central red YMB09 *GSMF* and the *HMF* complementary to the one associated to blue galaxies were used.

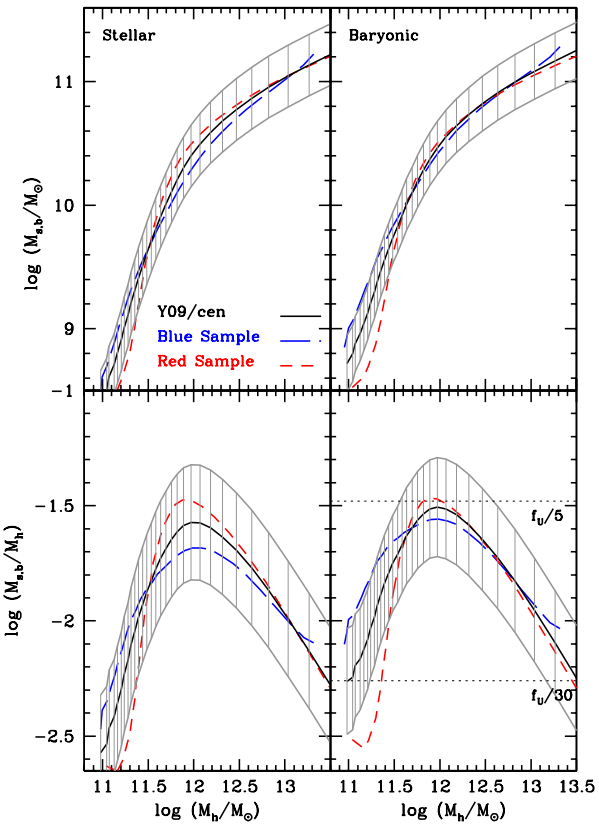

Fig. 5. Left panels: Mean $M_{\rm s}$–$M_{\rm h}$ (top) and $f_{\rm s}$–$M_{\rm h}$ (bottom) relations of all central (solid black line), blue central (long-dashed blue line), and red central (short-dashed red line) galaxies as inferred here using the YMB09 data. The grey curves connected by vertical lines show the 1σ uncertainty for the all-galaxies case; similar uncertainty regions around the main relations are found for the blue and red sub-samples (see Figure 8). Right panels: Same as in left panels but for $M_{\rm b}$ instead of $M_{\rm s}$. Dotted lines: $f_{\rm b} = f_U/5$ and $f_U/30$, where $f_U = 0.167$ is the universal baryon fraction. The color figure can be viewed online.

The shaded area in Figure 5 is the same 1σ uncertainty shown in Figure 4 for the overall central sample. The uncertainties corresponding to the $M_{\rm s}$–

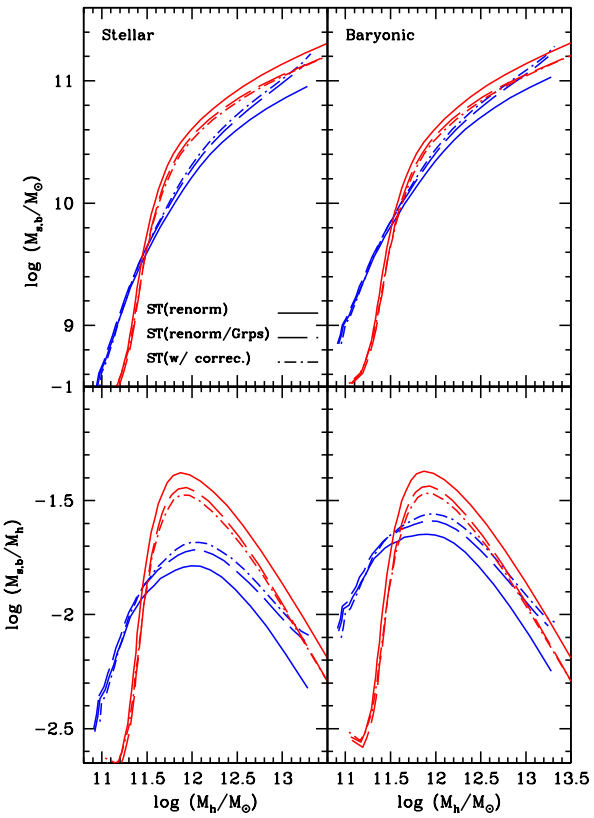

Fig. 6. Left panels: Mean M_s–M_h (top) and f_s–M_h (bottom) relations of central blue (blue lines) and red (red lines) galaxies when (i) no systematical corrections to the corresponding "blue" and "red" *HMF*s were applied apart from re-normalisations in the global abundance (see text, solid lines), (ii) the *HMF*s were corrected by group/cluster abundances and re-normalised (long-dashed lines), and (iii) the *HMF*s were corrected both by group/cluster abundances and late major mergers (as in Figure 4, dot-dashed lines). Right panels: Same as in left panels but for M_b instead of M_s. The color figure can be viewed online.

M_h and f_s–M_h relations for the blue and red galaxy sub-samples would be close to the one of the total sample if the corrections made to the *HMF* did not introduce an extra uncertainty. In fact this is not true, in particular for the group/cluster mass function introduced to correct the *HMF* associated to blue galaxies. Unfortunately, the work used for this correction does not report uncertainties. Hence, the uncertainties calculated here for the blue and red samples (shown explicitly in Figure 8 below) could be underestimated, specially at large masses.

In the mass range $11.5 \lesssim \log(M_h/M_\odot) \lesssim 13.0$, the M_s–M_h and f_s–M_h relations for central blue (red) galaxies lie slightly below (above) the relations corresponding to the overall sample. For masses below these ranges, the trends invert. The f_s–M_h curves for blue and red sub-samples peak at $\log(M_h/M_\odot) = 11.98$ and 11.87, with values of $f_s = 0.021^{+0.016}_{-0.009}$ and $f_s = 0.034^{+0.026}_{-0.015}$, respectively. The corresponding stellar masses at these peaks are $\log(M_s/M_\odot) = 10.30 \pm 0.25$ for blue galaxies and $\log(M_s/M_\odot) = 10.40 \pm 0.25$ for red galaxies. These masses are around 0.23 and 0.30 times the characteristic stellar mass $M^\star \approx 10^{10.93}\ M_\odot$ of the overall YMB09 *GSMF*, respectively. The maximum difference between the blue and red mean M_s–M_h relations is attained at $\log(M_h/M_\odot) \approx 11.9$; at this mass, the f_s value of the former is 1.7 times smaller than the f_s of the latter. For larger masses this difference decreases.

At the low-mass end, roughly $f_s \propto M_h$ ($\propto M_s^{0.5}$) and $f_s \propto M_h^{3.0}$ ($\propto M_s^{0.8}$) for the blue and red samples, respectively, while at the high-mass end, $f_s \propto M_h^{-0.4}$ ($\propto M_s^{-0.7}$) and $f_s \propto M_h^{-0.6}$ ($\propto M_s^{-1.5}$), respectively.

It is important to note that the differences between blue and red M_s–M_h relations at almost all masses are within the 1σ uncertainty of our inferences. We conclude that the M_s–M_h (f_s–M_h) relation does not depend significantly on galaxy color (type). If anything, the mean f_s–M_h relation of red galaxies is narrower and more peaked than the one of blue galaxies. In the mass range where the abundances of blue and red galaxies are closer ($10.0 < \log(M_s/M_\odot) < 10.7$), the intrinsic scatter around the M_s–M_h relation would slightly correlate with color in the sense that the redder (bluer) the galaxy, the larger (smaller) its M_s for a fixed M_h, with a maximum average deviation from the mean due to color no larger than ∼0.1 dex. For masses smaller than $M_s \approx 10^{9.7}\ M_\odot$, the correlation of the scatter with color would invert.

The (slight) differences between blue and red M_s–M_h (f_s–M_h) relations can be understood basically by the differences in the respective cumulative *GSMF*s and, at a minor level, by the differences of the corresponding *HMF*s for each case. The sharp peak in the red f_s–M_h relation is associated to the turn-over at $M_s \sim 10^{10.5}\ M_\odot$ in the *GSMF* of red galaxies (see Figure 1).

In order to estimate the influence of the corrections introduced to the *HMF* for blue (red) galaxies, we have redone the analysis using the original distinct (S-T) *HMF* without any correction but renormalised to obtain the same fraction of halos as the fraction implied by the *GSMF* of blue (red) galaxies with respect to the total *GSMF*. The results

TABLE 1

FIT PARAMETERS

Parameter	All	Blue	Red
$\log M_{0,h}$	11.97	11.99	11.87
$\log M_s^*$	10.40	10.30	10.40
β	0.34	0.37	0.18
α	1.45	0.90	1.50
γ	0.90	0.90	0.90
a $(M_s < M_s^*)$	0.000	0.125	0.000
a $(M_s > M_s^*)$	0.095	0.125	0.093

are shown in Figure 6, with solid curves of blue color (blue galaxies) and red color (red galaxies). For comparison, the corresponding relations plotted in Figure 5 are reproduced here (dot-dashed blue and red lines, respectively). One sees that the corrections to the *HMF* we have introduced for associating halos to the blue and red galaxy sub-samples act in the direction of reducing the differences among them in the $M_{\rm s}$–$M_{\rm h}$ ($f_{\rm s}$–$M_{\rm h}$) relations, specially for larger masses. The group/cluster mass function correction to the *HMF* hosting central blue galaxies is the dominant one. The dashed blue and red curves show such a case, where only this correction (and a small re-normalisation) is applied.

3.2.1. *Analytical fits to the stellar-halo mass relations*

From the comparison of the *GSMF* and *HMF* it is easy to deduce that high- and low-mass galaxies have significantly different $M_{\rm s}$–$M_{\rm h}$ scalings, a fact attributed to the different feedback/gas accretion mechanisms dominating in large and small systems (see e.g., Benson et al. 2003). The transition point between the low- and high-mass scalings defines a characteristic halo mass $M_{0,h}$ and an associated stellar mass M_s^*. Therefore, it was common to describe the $M_{\rm s}$–$M_{\rm h}$ relation as a double-power law with the turnover point at $M_{0,h}$. However, BCW10 have argued recently that a power-law at the high-mass side is conceptually a bad description for the $M_{\rm s}$–$M_{\rm h}$ relation and proposed a modification to it. Our results show indeed that a power-law is not sufficient to describe the high-mass side of the $M_{\rm s}$–$M_{\rm h}$ relations.

We have found that a good analytical description to the overall, blue, and red mean $M_{\rm s}$–$M_{\rm h}$ relations inferred here can be obtained for the inverse of the relations ($M_{\rm h}$ as a function of $M_{\rm s}$, as in BCW10), by proposing a power-law dependence for low masses and a sub-exponential law for high masses (see BCW10). The functional form that fits

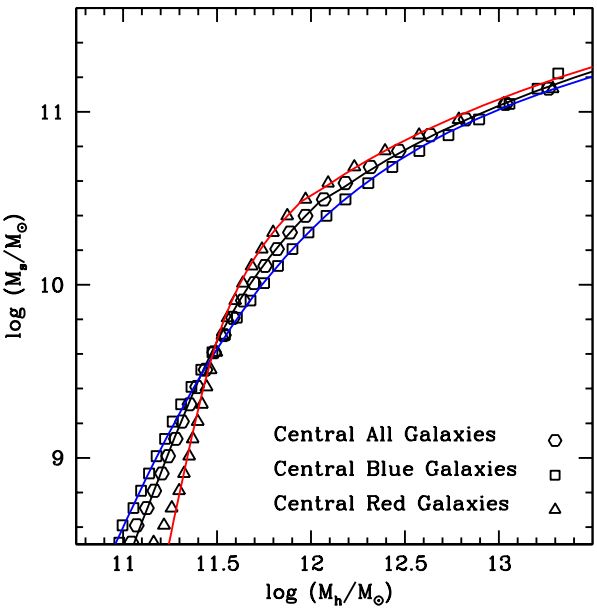

Fig. 7. Analytical fits given by equation (5) and Table 1 compared to the mean $M_{\rm s}$–$M_{\rm h}$ relation obtained here for all central galaxies (black solid line) and the central blue (blue solid line) and red (red solid line) galaxy subsamples. The color figure can be viewed online.

well the three $M_{\rm h}$–$M_{\rm s}$ relations is:

$$M_h = \frac{M_{0,h}}{2^\gamma}\left[\left(\frac{M_s}{M_s^*}\right)^{\beta/\gamma} + \left(\frac{M_s}{M_s^*}\right)^{\alpha/\gamma}\right]^\gamma 10^{a(M_s/M_s^*-1)}, \quad (5)$$

where β regulates the behavior of the relation at masses $M_{\rm s} < M_s^*$, α together with the sub-exponential term ($a < 1$) regulate the behavior at masses $M_{\rm s} > M_s^*$, and γ regulates the transition of the relation around M_s^*. In Table 1 are given the values of all the parameters that best fit our results for the (central) overall, blue, and red $M_{\rm s}$-$M_{\rm h}$ relations. Note that a assumes two different values depending on whether the mass is smaller or larger than M_s^*.

Figure 7 shows the three mean $M_{\rm s}$–$M_{\rm h}$ relations obtained here and the functional form given in equation (5) with the corresponding parameters reported in Table 1. The functional form is an excellent fit to the overall and blue $M_{\rm s}$–$M_{\rm h}$ relations at all masses and to the red $M_{\rm s}$–$M_{\rm h}$ relation for masses larger than $M_{\rm h} \approx 10^{11.3}\ M_\odot$.

3.3. *The baryonic-halo mass relations for central blue and red galaxies*

The right upper and lower panels of Figure 5 show the mean $M_{\rm b}$–$M_{\rm h}$ and $f_{\rm b}$–$M_{\rm h}$ relations, as in the left panels, for all central galaxies (solid line),

central blue (long-dashed blue line), and central red (short-dashed red line) galaxies. The blue and red *GBMF*s were calculated from the corresponding *GSMF*s and adding to $M_{\rm s}$ the respective gas mass, $M_{\rm g}$ (see § 2.1). The total *GBMF* is the sum of both of them. The error in $M_{\rm b}$ was calculated as the sum in quadrature of the errors in $M_{\rm s}$ and $M_{\rm g}$. This error, together with the intrinsic scatter in $M_{\rm s}$ (see § 2.2), both propagated to the $M_{\rm b}$–$M_{\rm h}$ relation, account for an uncertainty (standard deviation) of ∼0.23 dex in $\log M_{\rm b}$ at all masses (grey curves connected by vertical lines in Figure 5).

The baryonic mass fraction, $f_{\rm b}$, for blue galaxies is larger than the corresponding stellar one, $f_{\rm s}$, in particular at smaller halo masses. At $M_{\rm h} \approx 10^{11}\ M_{\odot}$, $f_{\rm b}$ is a factor 2.4 times higher than $f_{\rm s}$, while the peak of $f_{\rm b} = 0.028^{+0.018}_{-0.011}$ (at $M_{\rm h} = 10^{12.0}\ M_{\odot}$) is only 1.3 times larger than the peak of $f_{\rm s}$ (at $M_{\rm h} = 10^{12.0}\ M_{\odot}$). For larger masses, the difference between $f_{\rm b}$ and $f_{\rm s}$ decreases, while for smaller masses, the lower is $M_{\rm h}$, the larger is $f_{\rm b}$ compared to $f_{\rm s}$. For red galaxies, $f_{\rm s}$ and $f_{\rm b}$ are very similar, some differences being observed only at the lowest masses.

For masses larger (smaller) than $M_{\rm h} \approx 10^{11.6}\ M_{\odot}$, the differences between the $M_{\rm b}$–$M_{\rm h}$ ($f_{\rm b}$–$M_{\rm h}$) relation of blue and red galaxies become smaller (larger) than in the case of stellar masses (see § 3.2 and left panels of Figure 5). In general, the $f_{\rm b}$ bell-shaped curve for red galaxies is more peaked and narrower than the one for blue galaxies.

For blue galaxies, roughly $f_{\rm b} \propto {M_{\rm h}}^{0.7}$ (${M_{\rm b}}^{0.4}$) at the low-mass end, and $f_{\rm b} \propto {M_{\rm h}}^{-0.5}$ (${M_{\rm b}}^{-0.8}$) at the high-mass end. For red galaxies, roughly $f_{\rm b} \propto {M_{\rm h}}^{2.9}$ (${M_{\rm b}}^{0.8}$) at the low-mass end, and $f_{\rm b} \propto {M_{\rm h}}^{-0.6}$ (${M_{\rm b}}^{-1.5}$) at the high-mass end. For halos of masses $M_{\rm h} \approx 10^{11.0}\ M_{\odot}$ and $M_{\rm h} \approx 10^{13.2}\ M_{\odot}$, the baryon fraction for blue (red) galaxies decreases to values $f_{\rm b} \approx 0.004$ and 0.0085 ($f_{\rm b} \approx 0.0031$ and 0.0071), respectively. Therefore, for all masses, $f_{\rm b} \ll f_U$, where $f_U \equiv \Omega_b/\Omega_M$ is the universal baryon mass fraction; for the cosmology used here, $f_U = 0.167$.

4. DISCUSSION

4.1. *Comparison with other work*

As discussed in § 3.1 (see Figure 4), our inference of the local overall $M_{\rm s}$–$M_{\rm h}$ relation is in general in good agreement with several recent works that make use of the AMT (e.g., Baldry et al. 2008; Guo et al. 2010; Moster et al. 2010; BCW10). The aim in this paper is to estimate the $M_{\rm s}$–$M_{\rm h}$ and $M_{\rm b}$–$M_{\rm h}$ relations for blue (late-type) and red (early-type) central galaxies separately. We found that the differences between the means of the obtained relations for blue and red galaxies are within the 1σ uncertainty (see Figure 5). In more detail, the mean stellar and baryonic mass fractions ($f_{\rm s}$ and $f_{\rm b}$) as a function of $M_{\rm h}$ for red galaxies are narrower and more peaked than those for blue galaxies in such a way that for a given mass range (11.5–13.0 and 11.5–12.5 in $\log(M_{\rm h}/M_{\odot})$ for the stellar and baryonic cases, respectively) the former are higher than the latter, and outside these ranges the trend is inverted, especially at the low-mass side.

There are only a few previous attempts to infer the halo masses of central galaxies as a function of mass (luminosity) *and* galaxy type (Mandelbaum et al. 2006; More et al. 2011). These works use direct techniques (see Introduction), which are, however, limited by low signal-to-noise ratios, especially for less massive systems, so that the halo mass determinations are reliable only for galaxies with $M_{\rm s} \gtrsim 10^{10}\ M_{\odot}$. These techniques are galaxy-galaxy weak lensing and kinematics of satellite galaxies around central galaxies. In order to overcome the issue of low signal-to-noise ratios in the current measures, large samples of galaxies are stacked together in bins of similar properties (e.g., luminosity, $M_{\rm s}$, galaxy type) obtaining in this way higher (statistically averaged) signals of the corresponding measures (the tangential shear in the case of lensing and the weighted satellite velocity dispersion in the case of satellite kinematics). Besides, estimates of $M_{\rm h}$ with these sophisticated techniques are subject to several assumptions, among them, those related to the internal halo mass distribution. It is usual to assume the Navarro, Frenk, & White (1997) density profile with the mean concentration for a given mass as measured in N-body cosmological simulations.

It is not easy to achieve a fair comparison of the results obtained with the AM formalism and those with the direct methods. We have inferred the mean (and scatter) of $\log M_{\rm s}$ as a function of $M_{\rm h}$, while the weak lensing and satellite kinematics techniques constrain $M_{\rm h}$ as a function of $M_{\rm s}$ (see e.g., More et al. 2011); besides, the former calculates the mean of $M_{\rm h}$ (and its scatter) in a linear scale instead of a logarithmic one. These different ways of defining the relationship between stellar and halo masses, depending on the shapes and scatters of the corresponding relations, diverge less or more among them. In BCW10 (see their Figure 10), it was shown that at low masses ($\log(M_{\rm h}/M_{\odot}) \lesssim 12$, $\log(M_{\rm s}/M_{\odot}) \lesssim 10.5$), averaging $\log M_{\rm s}$ as a function of $M_{\rm h}$ or $\log M_{\rm h}$ as a function of $M_{\rm s}$ give equivalent results for the AMT, but at high masses, where the $M_{\rm s}$–$M_{\rm h}$ relation becomes much

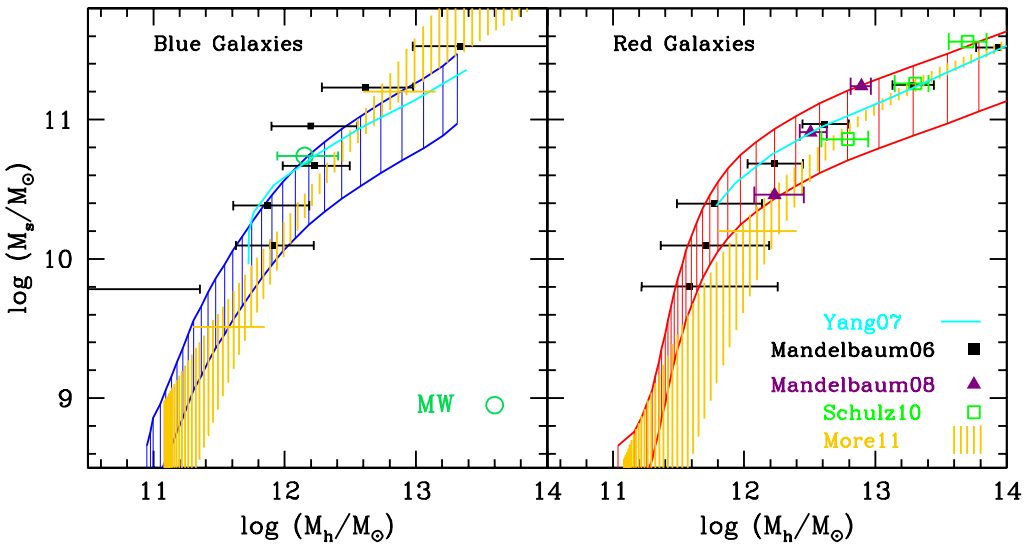

Fig. 8. Comparison with other observational inferences. Left panel: $M_{\rm s} - M_{\rm h}$ relation for blue (late-type) galaxies. The blue curves connected by vertical lines encompass the $\pm 1\sigma$ interval inferred here. We also reproduce the inferences using galaxy-galaxy weak lensing by Mandelbaum et al. (2006, black squares), galaxy groups (Yang et al. 2007, cyan solid line), and satellite kinematics (More et al. 2011, orange vertical lines). Estimates for the Milky Way are plotted (open circle with error bar). Right panel: $M_{\rm s} - M_{\rm h}$ relation for red (early-type) galaxies. The red curves connected by vertical lines encompass the $\pm 1\sigma$ interval inferred here. Other determinations as in the left panel but for early-type galaxies are plotted. More recent inferences with the weak lensing technique by Mandelbaum et al. (2008, filled violet triangles) and by Schulz et al. (2010, open green squares) are also plotted. The color figure can be viewed online.

shallower, this relation becomes steeper (higher stellar mass at a fixed halo mass) for the latter case with respect to the former one.

In Figure 8, the results from Mandelbaum et al. (2006) are reproduced, left panel for central late-type galaxies and right panel for central early-type galaxies (solid squares with error bars). The error bars are 95 percent confidence intervals (statistical). Mandelbaum et al. (2006) have used the (de Vaucouleours/exponential) bulge-to-total ratio, frac_deV, given in the SDSS PHOTO pipeline as a criterion for late- (frac_deV<0.5) and early-type (frac_dV≥ 0.5) separation. This criterion of course is not the same as the color used in YMB09, but there is a correlation between both of them in such a way that a comparison between our results and those of Mandelbaum et al. (2006) is qualitatively possible. Note that we have decreased the halo masses of Mandelbaum et al. (2006) by $\approx$15% on going from their to our definition of halo virial mass. In more recent works, Mandelbaum, Seljak, & Hirata (2008) and Schulz, Mandelbaum, & Padmanabhan (2010) reported a new weak lensing analysis for the massive central early-type galaxies using the seventh SDSS data release (DR7) and a more sophisticated criteria for selecting the early-type lens population. Their results are plotted in the right panel of Figure 8 with solid triangles and open squares, respectively.

In the case of the satellite kinematics determinations of $M_{\rm h}$ by More et al. (2011), the same SDSS sample and similar recipes as in YMB09 for calculating $M_{\rm s}$, classifying galaxies into blue and red, and finding central and satellites galaxies were used. More et al. (2011) applied their analysis to constrain the mean $\log M_{\rm h}$ as a function of $M_{\rm s}$, but also presented the constraints of their model for the mean of $\log M_{\rm s}$ as a function of $M_{\rm h}$. Their results for the latter case, kindly made available to us in electronic form by Dr. S. More, are reproduced in Figure 8 as the shaded (orange) regions which represent the 68% confidence intervals. On going from their to our definitions of halo mass and IMF, their $M_{\rm h}$ and $M_{\rm s}$ were decreased by $\approx$15% and $\approx$25%, respectively. The dotted horizontal lines in each panel show the approximate range in $M_{\rm s}$ where the determinations are reliable according to More et al. (2011, see their Figure 11).

In More et al. (2011) are also reported results for the average $M_{\rm h}$ as a function of $M_{\rm s}$ split into central blue and red galaxies corresponding to the galaxy group analysis by Yang et al. (2007). The solid (cyan) curves in Figure 8 reproduce these results.

Finally, the standard $\pm 1\sigma$ deviation intervals that we have obtained from the AMT are reproduced in Figure 8 for central blue and red galaxies (solid blue and red curves connected by vertical lines, respectively). Note that in the determinations with direct methods, the systematic uncertainty in $M_{\rm s}$, which is the main source of error in the AMT, was not taken into account.

Our inference for early-type (red) galaxies is consistent (within the uncertainties, errors, and different ways of presenting the constraints) with the weak lensing results of Mandelbaum et al. (2006) and Schulz et al. (2010), and with the galaxy group analysis of Yang et al. (2007) as reported in More et al. (2011), for all the masses reported in each one of these papers. With respect to the satellite kinematics analysis by More et al. (2011), their mean halo masses for $M_{\rm s} \sim 5 \times 10^9 - 10^{11}\ M_\odot$ (for smaller masses their uncertainties are very large) are larger than ours (and those of Mandelbaum et al. 2006) by factors around 2. For larger masses, all determinations agree roughly with our results. In fact, there is some indication that satellite kinematics yields halo masses around low mass central galaxies that are systematically larger than most other methods, specially for red central galaxies (Skibba et al. 2011; but see More et al. 2011 for a discussion).

For late-type (blue) galaxies, our results are in reasonable agreement with those of Mandelbaum et al. (2006) for masses $M_{\rm s} \lesssim 10^{10.8}\ M_\odot$. At higher masses, their results imply halo masses for a given $M_{\rm s}$ smaller than ours, with the difference increasing with increasing stellar mass. The discrepancy would be weaker taking into account that the mean $M_{\rm s}$–$M_{\rm h}$ relation in our case becomes steeper when calculating $M_{\rm h}$ as a function of $M_{\rm s}$. On the other hand, it must be said that the number statistics becomes poor for massive late-type galaxies, resulting in a stacked weak lensing analysis with large error bars. For example, in the two most massive bins in the Mandelbaum et al. (2006) sample (the two uppermost points in Figure 8), only 5 and 11 percent of the galaxies are classified as late types. Future weak lensing work should confirm whether high-mass late-type galaxies do or do not have such relatively small halos as found in Mandelbaum et al. (2006). Regarding the comparison with the satellite kinematics inferences of More et al. (2011), the agreement is reasonable at least up to $M_{\rm s} \approx 10^{11}\ M_\odot$, though the relation inferred by these authors is less curved than ours. For larger masses, these authors caution that their results become very uncertain, as in the weak lensing case, because of poor statistics of massive blue galaxies. The galaxy groups inference (Yang et al. 2007), in the mass range allowed by this technique, gives halo masses slightly smaller than the means of our inference for a given $M_{\rm s}$.

In general, most techniques for inferring the relationship between stellar and halo masses of galaxies agree among them within factors up to 2–3 in $M_{\rm h}$ (BCW10; More et al. 2011; Dutton et al. 2010). This seems to be also the case for samples partitioned into late- and early-type galaxies, as shown here. However, beyond the detailed comparison between our results and those obtained with direct techniques, it seems that there is a systematic qualitative difference: in our case, at a given halo mass (for $10^{11.5}\ M_\odot \lesssim M_{\rm h} \lesssim 10^{13.0}\ M_\odot$), blue centrals, on average, have lower stellar masses than red centrals, while in the case of determinations with direct techniques, the opposite occurs, at least for masses larger than $M_{\rm h} \sim 10^{12}\ M_\odot$ (Mandelbaum et al. 2006; More et al. 2011; see also Figures 5 and 8).

A partial source of bias contributing to this difference could be that in the weak lensing and satellite kinematics techniques the same concentration for halos hosting late- and early-type galaxies is assumed. If halos of late- (early-)type galaxies are less (more) concentrated than the corresponding average, then for the same measure (shear or satellite velocity dispersion), the halo masses are expected to be higher (lower) than the obtained ones. Therefore, the differences found (Mandelbaum et al. 2006 and More et al. 2011) in the mass halos of late- and early-type galaxies of a given $M_{\rm s}$ would decrease or even invert their sense.

While it is difficult to make any robust statement about possible systematics in each technique regarding late and early types, we ask ourselves what should be modified in our assumptions in order to invert the behavior of the $M_{\rm s}$–$M_{\rm h}$ relations with galaxy type (color) obtained here. We have shown in Figure 6 that our corrections to the *HMF* had the effect of bringing the $M_{\rm s}$–$M_{\rm h}$ relations of blue and red galaxies into closer agreement at large masses. One possibility in order not only to bring the relations into closer agreement but to invert them is to make even steeper (shallower) the *HMF* corresponding to blue (red) galaxies, mainly at the high-mass end (see Figure 3, lower panel). This would imply, for instance, a larger correction to the *HMF* due to groups than that made by us. The group/cluster mass function used by us (Heinämäki et al. 2003) is one of the most general ones found in the literature; it includes all kinds of groups/clusters with 3 or more members and $\delta N/N \geq 80$. The authors note that their sam-

ple is complete down to a dynamical mass roughly equivalent to $M_{\rm h} = 5\times10^{13}\ M_{\odot}$. It could be that the abundance of groups of lower masses is larger than that given in Heinämäki et al. (2003), though it is difficult to accept that blue galaxies are completely absent in the centers of small and loose groups of a few (> 2) members.

Last but not least, in Figure 8 we include observational estimates for our Galaxy (open circle). The uncertainties in the estimates of $M_{\rm h}$ for the Milky Way are still large but better than most of the determinations for other individual galaxies. For recent reviews on different results see Guo et al. (2010) and Dutton et al. (2010). In Figure 8 we plot a recent estimate of $M_{\rm h}$ based on observations of 16 high velocity stars (Smith et al. 2007). These authors find $M_{\rm h} = 1.42^{+1.14}_{-0.54} \times 10^{12}\ M_{\odot}$, which is in good agreement with several previous works (e.g., Wilkinson & Evans 1999; Sakamoto, Chiba, & Beers 2003; Li & White 2008), though results from Xue et al. (2008) suggest lower values (but see a recent revision by Przybilla et al. 2010). For its $M_{\rm h}$, the $M_{\rm s}$ of the Milky Way seems to be at the high extremum of blue galaxies, close to values typical of red galaxies. It should be said that it is an open question whether the Milky Way is an average galaxy or not. In the stellar Tully-Fisher and radius–$M_{\rm s}$ relations (e.g., Avila-Reese et al. 2008), the Milky Way is shifted from the average to the high-velocity and low-radius sides, respectively.

4.2. *Interpretations and consistency of the results*

Although our main result is that the differences between the $M_{\rm s}$–$M_{\rm h}$ and $M_{\rm b}$–$M_{\rm h}$ relations for central blue and red galaxies are marginal (within the uncertainties of our determinations), we will explore whether such differences are expected or not. For this it is important to approach the problem from an evolutionary point of view.

In Firmani & Avila-Reese (2010, hereafter FA10), the determinations of the $M_{\rm s}$–$M_{\rm h}$ relation for all galaxies at different redshifts, out to $z = 4$ (BCW10), and the average ΛCDM individual halo mass aggregation histories (MAHs) were used to determine the individual *average* $M_{\rm s}$ growth of galaxies in general as a function of mass (called in that paper as Galaxian Hybrid Evolutionary Tracks, GHETs). It was found that the more massive the galaxies, the earlier transit from their active (star-forming, blue) regime of $M_{\rm s}$ growth to a passive (red) phase (population 'downsizing'), while their corresponding halos continue growing, more efficiently at later epochs the more massive they are ('upsizing'). The inferred trend for the transition stellar mass is $\log(M_{\rm tran}/M_{\odot}) \approx 10.30 + 0.55z$. Therefore, galaxies of mass $M_{\rm s} \approx 10^{10.3}\ M_{\odot}$ are on average becoming passive (red) today. For $M_{\rm s} \gtrsim M_{\rm tran}$, the larger the mass, the redder will be the galaxy on average. The opposite applies for $M_{\rm s} \lesssim M_{\rm tran}$, the smaller the mass, the bluer will be the galaxy. Interestingly enough, $M_{\rm s} \approx 10^{10.3}\ M_{\odot}$ is roughly the mass where the overall YMB09 blue and red *GSMF*s cross: for masses larger than this crossing mass, $M_{\rm cross}$, redder galaxies become more and more abundant than bluer ones and the inverse happens at smaller masses (see Figure 1).

Galaxies that are transiting from active to passive at $z \sim 0$ (those around $M_{\rm tran} \approx 10^{10.3}\ M_{\odot}$) have probably been subject recently to a process that induced an *efficient* transformation of the available gas into stars in such a way that their stellar populations started to redden passively. Hence, for a given $M_{\rm h}$, they are expected to have a higher $M_{\rm s}$ (or $f_{\rm s}$) than those galaxies of similar mass that did not suffer (yet?) the above process (bluer ones). The relatively small difference in $f_{\rm s}$ for blue and red galaxies we have found here (whose maximum is attained around $M_{\rm tran} \sim M_{\rm cross}$, Figure 5) would imply that the scatter around $M_{\rm tran}$ is moderate.

Galaxies more massive than $M_{\rm tran}$ (or $M_{\rm cross}$), according to the evolutionary analysis by FA10, underwent the process of efficient gas consumption into stars (and the further cessation of $M_{\rm s}$ growth) earlier on average than more massive galaxies, while their halos continue growing. Therefore, one expects that the more massive the galaxy, the redder and the lower its stellar (and baryonic) mass fraction $f_{\rm s}$ will be on average. The few blue massive galaxies may have slightly smaller stellar masses (lower $f_{\rm s}$) than the corresponding red ones because they should have transformed gas into stars less efficiently in the past. Therefore, by including gas, i.e. when passing to $f_{\rm b}$ the difference between blue and red massive galaxies at large masses should become negligible. This is indeed what happens (see Figure 5).

Galaxies less massive than $M_{\rm tran}$ (or $M_{\rm cross}$) at $z \sim 0$, according to FA10, are in general the more actively assembling their stellar masses the smaller they are ('downsizing' in specific SFR), while their dark halo mass growth is already very slow. This implies the existence in the galaxies of relatively larger reservoirs of cold gas the smaller they are (gas not related to the halo-driven infall) because the SF has been delayed in the disk and/or cold gas is being lately (re)accreted into the galaxy. However, if for some reason the gas reservoir in these galaxies is lost,

then the galaxy will redden and its baryonic and stellar mass fractions will be smaller than those of the galaxies that were able to keep their gas reservoir (the majority), in agreement with our inferences here (Figure 5).

5. SUMMARY AND CONCLUSIONS

By means of the AM technique and using the central blue and red *GSMF*s, constructed from the local SDSS sample by YMB09, we have inferred the local $M_{\rm s}$–$M_{\rm h}$ (or $f_{\rm s}$–$M_{\rm h}$) relations for *central* galaxies and for the sub-samples of blue and red galaxies. To derive the relations for the sample of blue galaxies, (i) the mass function of observed groups/clusters of galaxies is subtracted from the distinct (S-T) *HMF* (blue, late-type galaxies are not observed in the centers of groups and clusters), and (ii) halos that suffered a major merger since $z = 0.8$ are excluded. For red galaxies, the *HMF* is assumed to be the complement of the "blue" one, with respect to the overall (distinct) *HMF*. We consider as sources of uncertainty in our analysis only the systematical error in assigning stellar masses to galaxies (0.25 dex) and the intrinsic statistical scatter in stellar mass at a fixed halo mass (0.16 dex). By using the observational $M_{\rm g}$–$M_{\rm s}$ relation and its scatter, we transited from $M_{\rm s}$ to $M_{\rm b}$ (= $M_{\rm s}$+ $M_{\rm g}$) in the *GSMF* and estimated the overall blue and red *GBMF*s, which were used to obtain the corresponding baryonic $M_{\rm b}$–$M_{\rm h}$ (or $f_{\rm b}$–$M_{\rm h}$) relations using the AM technique.

The $M_{\rm s}$–$M_{\rm h}$ relation obtained here agrees rather well with previous studies (see Figure 4). The small differences found in this work can be explained mainly in terms of the different *GSMF*s used in each study, and to a lesser extent by variations in the methodology. The 1σ uncertainty in the obtained $M_{\rm s}$–$M_{\rm h}$ relation is ≈ 0.25 dex in log $M_{\rm s}$. The $M_{\rm s}$–$M_{\rm h}$ relation of central galaxies lies below (lower $M_{\rm s}$ for a given $M_{\rm h}$) the overall one by a factor ~ 1.6 at $M_{\rm h} = 10^{11}\ M_\odot$ and by less than 5% for $M_{\rm h} > 10^{13}\ M_\odot$.

Our main result refers to the calculation of the *central* $M_{\rm s}$–$M_{\rm h}$ and $M_{\rm b}$–$M_{\rm h}$ relations for the two broad populations into which the galaxy sample can be divided: blue (late-type) and red (early-type) galaxies. We highlight the following results from our analysis:

• At $M_{\rm h} \gtrsim 10^{11.3}\ M_\odot$ the mean stellar mass fraction $f_{\rm s}$ of blue galaxies is smaller than that of red galaxies, the maximum difference being attained at $M_{\rm h} \approx 10^{11.7}\ M_\odot$; at this mass, the $f_{\rm s}$ of red galaxies is 1.7 times that of blue galaxies (see Figure 5). At larger masses, the difference decreases until it disappears. At $M_{\rm h} \lesssim 10^{11.3}\ M_\odot$ the trend is reversed as blue galaxies tend to have higher values of $f_{\rm s}$ than red ones. In the case of the baryonic mass fractions, $f_{\rm b}$, the same trends of the stellar relations remain but at $M_{\rm h} \gtrsim 10^{11.3}\ M_\odot$ the difference in $f_{\rm b}$ between blue and red galaxies is small, while for smaller masses, the difference increases.

• The $M_{\rm s}$–$M_{\rm h}$ and $M_{\rm b}$–$M_{\rm h}$ (or $f_{\rm s}$–$M_{\rm h}$ and $f_{\rm b}$–$M_{\rm h}$) relations of central blue and red sub-samples do not differ significantly from the respective relations of the overall central sample, and these differences are within the 1σ uncertainty of the inferences (Figure 5). For blue (red) galaxies, the maximum value of $f_{\rm s}$ is $0.021^{+0.016}_{-0.009}$ ($0.034^{+0.026}_{-0.015}$) and is attained for halos of mass $M_{\rm h} = 10^{11.98}\ M_\odot$ ($M_{\rm h} = 10^{11.87}\ M_\odot$); the corresponding stellar mass is $M_{\rm s} = 10^{10.30\pm0.25}\ M_\odot$ ($M_{\rm s} = 10^{10.40\pm0.25}\ M_\odot$), which is around 0.23 (0.30) times $M^\star$, the Schechter fit characteristic mass of the overall *GSMF* of YMB09. For smaller and larger masses, $f_{\rm s}$ significantly decreases.

• We have compared our results with the few observational inferences of the $M_{\rm s}$–$M_{\rm h}$ relation for blue (late-type) and red (early-type) galaxies that exist in the literature. Although these studies estimate halo masses using direct techniques (weak lensing and galaxy satellite kinematics), they are still limited by the stacking approach they need to apply (due to the low signal-to-noise ratio of individual galaxies) and by the large uncertainties owing to the unknown systematics. The overall differences among the different studies (including ours) amount to factors of up to 2–4 at a given mass (these factors being much smaller at other masses) for most methods (Figure 8). For blue galaxies, all methods agree reasonably well for low masses ($M_{\rm h} \lesssim 3 \times 10^{12}\ M_\odot$), but for higher masses, our inference implies larger halos for a given $M_{\rm s}$ than the results from direct techniques. For red galaxies, at high masses ($M_{\rm h} \gtrsim 3 \times 10^{12}\ M_\odot$), all methods agree reasonably well, but at lower masses, the satellite kinematics technique produces halo masses, for a given $M_{\rm s}$, larger than those obtained by other methods.

• According to our results, for $M_{\rm h} \lesssim 10^{11.3}\ M_\odot$, the intrinsic scatter of the $M_{\rm s}$–$M_{\rm h}$ relation should slightly anti-correlate with galaxy color (for a fixed $M_{\rm h}$, the bluer the galaxy, the higher its $M_{\rm s}$), while for more massive systems, the correlation should be direct (for a fixed $M_{\rm h}$, the redder the galaxy, the higher its $M_{\rm s}$). For massive blue galaxies to have had higher higher $f_{\rm s}$ values than red ones as the results from direct techniques suggest, the *HMF* halos hosting blue (red) galaxies should have been even steeper

(shallower) than what we have proposed here; this seems too extreme.

• The maximum baryon mass fraction of blue and red galaxies are $f_{\rm b} = 0.028^{+0.018}_{-0.011}$ and $f_{\rm b} = 0.034^{+0.025}_{-0.014}$, respectively, much smaller than $f_U = 0.167$ in both cases, and these maxima are attained at $M_{\rm h} \approx 10^{12}\ M_\odot$. At large masses $f_{\rm b}$ decreases approximately as $f_{\rm b} \propto {M_{\rm h}}^{-0.5}({M_{\rm b}}^{-0.8})$ for blue galaxies and as $f_{\rm b} \propto {M_{\rm h}}^{-0.6}({M_{\rm b}}^{-1.5})$ for red galaxies, in such a way that from $M_{\rm h} \approx 5 \times 10^{12}\ M_\odot$ on, blue galaxies have on average slightly larger values of $f_{\rm b}$ than red ones. At low masses, the $f_{\rm b}$ of red galaxies strongly decreases as the mass decreases $f_{\rm b} \propto {M_{\rm h}}^{2.9}({M_{\rm b}}^{0.8})$, while for blue galaxies, due to the increasing gas fractions the smaller the mass, $f_{\rm b}$ decreases more slowly than $f_{\rm s}$, as $f_{\rm b} \propto {M_{\rm h}}^{0.7}$ $(\propto {M_{\rm b}}^{0.4})$.

The AM technique has been revealed as a relatively simple but powerful method for connecting empirically galaxies to dark halos. Here we extended this technique towards inferences for the blue and red galaxy sub-populations separately. By introducing a minimum of assumptions –otherwise the method becomes close to a semi-analytical model– we have found that the stellar and baryon mass-halo mass relations of blue and red galaxies do not differ significantly among them and from the overall ones. The maximum differences occur around the peak of these relations, $M_{\rm h} \approx 10^{12}\ M_\odot$, and are consistent qualitatively with the inference that the galaxies in these halos are transiting from an active to a quiescent regime of $M_{\rm s}$ growth (FA10). Those that transited recently did so because they had an efficient process of gas consumption into stars and further cessation of $M_{\rm s}$ growth; therefore, they should be redder and have higher $f_{\rm s}$ values than those that have not transited. For larger and smaller masses than $M_{\rm h} \approx 10^{12}\ M_\odot$, the differences decrease and even invert, something that is also consistent with the inferences by FA10, based on the semi-empirical determinations of the evolution of the overall $M_{\rm s}$–$M_{\rm h}$ relation.

We thank the referee for his/her useful comments and suggestions. We are grateful to Dr. S. More for sending us in electronic form the data plotted in Figure 8. A.R-P. acknowledges a graduate student fellowship provided by Conacyt. We thank PAPIIT-Universidad Nacional Autónoma de México grant IN114509 and Conacyt grant 60354 for partial funding, as well as a bilateral DFG-Conacyt grant through which we got access to results from N-body numerical simulations performed by Dr. S. Gottloeber.

REFERENCES

Avila-Reese, V. 2007, in Ap&SS Proc., Stellar and Galactic Connections Between Particle Physics and Astrophysics, ed. A. Carramiñana et al. (Berlin: Springer), 115 (arXiv:astro-ph/0605212v1)
Avila-Reese, V., Zavala, J., Firmani, C., & Hernández-Toledo, H. M. 2008, AJ, 136, 1340
Baldry, I. K., Balogh, M. L., Bower, R. G., Glazebrook, K., Nichol, R. C., Bamford, S. P., & Budavari, T. 2006, MNRAS, 373, 469
Baldry, I. K., Glazebrook, K., & Driver, S. P. 2008, MNRAS, 388, 945
Baugh, C. M. 2006, Rep. Prog. Phys., 69, 3101
Behroozi, P. S., Conroy, C., & Wechsler, R. H. 2010, ApJ, 717, 379 (BCW10)
Bell, E. F., McIntosh, D. H., Katz, N., & Weinberg, M. D. 2003, ApJS, 149, 289
Benson, A. J. 2010, Phys. Rep., 495, 33
Benson, A. J., Bower, R. G., Frenk, C. S., Lacey, C. G., Baugh, C. M., & Cole, S. 2003, ApJ, 599, 38
Berlind, A. A., & Weinberg, D. H. 2002, ApJ, 575, 587
Bernardi, M., Shankar, F., Hyde, J. B., Mei, S., Marulli, F., & Sheth, R. K. 2010, MNRAS, 404, 2087
Blanton, M. R., & Moustakas, J. 2009, ARA&A, 47, 159
Boylan-Kolchin, M., Ma, C.-P., & Quataert, E. 2008, MNRAS, 383, 93
Chabrier, G. 2003, PASP, 115, 763
Cole, S., et al. 2001, MNRAS, 326, 255
Conroy, C., Gunn, J. E., & White, M. 2009, ApJ, 699, 486
Conroy, C., & Wechsler, R. H. 2009, ApJ, 696, 620
Conroy, C., Wechsler, R. H., & Kravtsov, A. V. 2006, ApJ, 647, 201
de Lapparent, V., & Slezak, E. 2007, A&A, 472, 29
Dutton, A. A., Conroy, C., van den Bosch, F. C., Prada, F., & More, S. 2010, MNRAS, 407, 2
Dutton, A. A., & van den Bosch, F. C. 2009, MNRAS, 396, 14
Dutton, A. A., van den Bosch, F. C., Dekel, A., & Courteau, S. 2007, ApJ, 654, 27
Firmani, C., & Avila-Reese, V. 2000, MNRAS, 315, 457
_____. 2010, ApJ, 723, 755 (FA10)
Gallazzi, A., & Bell, E. F. 2009, ApJS, 185, 253
Giocoli, C., Tormen, G., Sheth, R. K., & van den Bosch, F. C. 2010, MNRAS, 404, 502
Gnedin, O. Y., Weinberg, D. H., Pizagno, J., Prada, F., & Rix, H.-W. 2007, ApJ, 671, 1115
Governato, F., Mayer, L., & Brook, C. 2008, in ASP Conf. Ser. 396, Formation and Evolution of Galaxy Disks, ed. J. G. Funes, S. J., & E. M. Corsini (San Francisco: ASP), 453
Guo, Q., White, S., Li, C., & Boylan-Kolchin, M. 2010, MNRAS, 367
Heinämäki, P., Einasto, J., Einasto, M., Saar, E., Tucker, D. L., & Müller, V. 2003, A&A, 397, 63

Komatsu, E., et al. 2009, ApJS, 180, 330
Kravtsov, A. V., Berlind, A. A., Wechsler, R. H., Klypin, A. A., Gottlöber, S., Allgood, B., & Primack, J. R. 2004, ApJ, 609, 35
Li, C., Kauffmann, G., Jing, Y. P., White, S. D. M., Börner, G., & Cheng, F. Z. 2006, MNRAS, 368, 21
Li, C., & White, S. D. M. 2009, MNRAS, 398, 2177
Li, Y.-S., & White, S. D. M. 2008, MNRAS, 384, 1459
Mandelbaum, R., Seljak, U., & Hirata, C. M. 2008, JCAP, 8, 6
Mandelbaum, R., Seljak, U., Kauffmann, G., Hirata, C. M., & Brinkmann, J. 2006, MNRAS, 368, 715
Marinoni, C., & Hudson, M. J. 2002, ApJ, 569, 101
Martínez, H. J., Zandivarez, A., Merchán, M. E., & Domínguez, M. J. L. 2002, MNRAS, 337, 1441
McGaugh, S. S. 2005, ApJ, 632, 859
Mo, H.J., Mao, S., & White, S.D.M. 1998, MNRAS, 295,319
More, S., van den Bosch, F. C., Cacciato, M., Mo, H. J., Yang, X., & Li, R. 2009, MNRAS, 392, 801
More, S., van den Bosch, F. C., Cacciato, M., Skibba, R., Mo, H. J., & Yang, X. 2011, MNRAS, 410, 210
Moster, B. P., Somerville, R. S., Maulbetsch, C., van den Bosch, F. C., Macciò, A. V., Naab, T., & Oser, L. 2010, ApJ, 710, 903
Navarro, J. F., Frenk, C. S., & White, S. D. M. 1997, ApJ, 490, 493
Norberg, P., et al. 2001, MNRAS, 328, 64
Padilla, N., Lambas, D. G., & González, R. 2010, MNRAS, 409, 936
Peacock, J. A., & Smith, R. E. 2000, MNRAS, 318, 1144
Press, W. H., & Schechter, P. 1974, ApJ, 187, 425
Przybilla, N., Tillich, A., Heber, U., & Scholz, R.-D. 2010, ApJ, 718, 37
Robertson, B., Yoshida, N., Springel, V., & Hernquist, L. 2004, ApJ, 606, 32
Sakamoto, T., Chiba, M., & Beers, T. C. 2003, A&A, 397, 899
Schulz, A. E., Mandelbaum, R., & Padmanabhan, N. 2010, MNRAS, 408, 1463
Shankar, F., Lapi, A., Salucci, P., De Zotti, G., & Danese, L. 2006, ApJ, 643, 14
Shao, Z., Xiao, Q., Shen, S., Mo, H. J., Xia, X., & Deng, Z. 2007, ApJ, 659, 1159
Sheth, R. K., & Tormen, G. 1999, MNRAS, 308, 119 (S-T)
Skibba, R. A., van den Bosch, F. C., Yang, X., More, S., Mo, H., & Fontanot, F. 2011, MNRAS, 410, 417
Smith, M. C., et al. 2007, MNRAS, 379, 755
Stewart, K. R., Bullock, J. S., Barton, E. J., & Wechsler, R. H. 2009, ApJ, 702, 1005
Stringer, M. J., & Benson, A. J. 2007, MNRAS, 382, 641
Tinker, J., et al. 2008, ApJ, 688, 709
Tucker, D. L., et al. 2000, ApJS, 130, 237
Vale, A., & Ostriker, J. P. 2004, MNRAS, 353, 189
van den Bosch, F. C. 2000, ApJ, 530, 177
Wang, L., & Jing, Y. P. 2010, MNRAS, 402, 1796
Wang, Y., et al. 2009, ApJ, 697, 247
Wei, L. H., Kannappan, S. J., Vogel, S. N., & Baker, A. J. 2010, ApJ, 708, 841
Weinmann, S. M., van den Bosch, F. C., Yang, X., & Mo, H. J. 2006, MNRAS, 366, 2
Wilkinson, M. I., & Evans, N. W. 1999, MNRAS, 310, 645
White, S. D. M., & Frenk, C. S. 1991, ApJ, 379, 52
White, S. D. M., & Rees, M. J. 1978, MNRAS, 183, 341
Xue, X. X., et al. 2008, ApJ, 684, 1143
Yang, X., Mo, H. J., Jing, Y. P., van den Bosch, F. C., & Chu, Y. 2004, MNRAS, 350, 1153
Yang, X., Mo, H. J., & van den Bosch, F. C. 2003, MNRAS, 339, 1057
_____. 2008, ApJ, 676, 248
_____. 2009, ApJ, 695, 900 (YMB09)
Yang, X., Mo, H. J., van den Bosch, F. C., Pasquali, A., Li, C., & Barden, M. 2007, ApJ, 671, 153
Zehavi, I., et al. 2005, ApJ, 630, 1

A. Rodríguez-Puebla & V. Avila-Reese: Instituto de Astronomía, Universidad Nacional Autónoma de México, Apdo. Postal 70-264, 04510, México, D.F., Mexico (apuebla@astroscu.unam.mx).
C. Firmani: Osservatorio Astronomico di Brera, via E.Bianchi 46, I-23807 Merate, Italy.
P. Colín: Centro de Radioastronomía y Astrofísica, Universidad Nacional Autónoma de México, Apdo. Postal 72-3 (Xangari), Morelia, Michoacán 58089, Mexico.